Acta Geochim (2025) 44:784–804
https://doi.org/10.1007/s11631-024-00755-6

ORIGINAL ARTICLE

Magma heterogeneity in the generation of ophiolitic mafic rocks on the eastern flank of the Indian plate

Sashimeren Imtisunep[1] · Athokpam Krishnakanta Singh[1,2] · Monika Chaubey[1] · Rajkumar Bikrmaditya Singh[3] · Bendangtola Longchar[4] · Shoraisam Khogenkumar[5] · Amrita Dutt[6]

Received: 11 June 2024 / Revised: 23 December 2024 / Accepted: 29 December 2024 / Published online: 31 January 2025

Abstract Subduction polarity reversal typically occurs in intra-oceanic arc settings; the existence of an ancient intra-oceanic arc and its associated back-arc system within the Neotethyan plate has been deliberated. In this study, we investigate the possible role of subduction initiation of polarity reversal in the formation of Nagaland-Manipur ophiolite (NMO), evaluate the petrological and geochronological data and compare it with the neighboring natural examples of subduction polarity reversal of the Andaman-Nicobar ophiolite (ANO). The ancient intra-oceanic arc, namely the Incertus-Woyla Arc, and its associated back-arc remnant have been correlated with the back-arc mafic of the ANO. We found that the geochemical signatures of mafic rocks of NMO and ANO are comparable, and the available geochronology data of ~ 145 Ma from the NMO basalt and chert fit well with the evolution and formation of the intra-oceanic arc, i.e., Incertus-Woyla Arc. The evolution and age of the Incertus-Woyla Arc are between 135 and 150 Ma. Although the oldest age of the ANO has been reported from metamorphic sole at about 106.4 and 105.3 Ma, the back-arc affinity of the amphibole has been credited to the back-arc spreading that occurred behind the Woyla Arc. Previous paleomagnetic and geochronological studies have suggested that the development of the back-arc basin behind the Incertus-Woyla Arc was a result of divergent double subduction. Therefore, we have inferred a similar scenario for the development of the back-arc affinity rocks of the NMO behind the Incertus-Woyla Arc and the reinterpretation for the evolution of the supra-subduction zone affinity rocks of NMO and ANO during subduction initiation after subduction polarity reversal.

Keywords Geochemistry · Basalt · Intra-oceanic · Back arc · Subduction polarity reversal · Ophiolites · Northeast India

1 Introduction

Ophiolites are fossilized remains of oceanic crust, which are widely studied to understand the ancient subduction zones. Although the development of ophiolite could be initiated at various tectonic settings like the mid-oceanic ridge, supra-subduction zone, and within-plate environment, a large portion of it was generated in the supra-subduction zone (Pearce 2008; Dilek and Furnes 2011; Singh 2013). The sinking of oceanic lithosphere at the subduction zone triggers the closure of oceanic basins, connects Earth's exterior with its interior, continental crust collision, and felsic and mafic magmatism along the suture zone (Harris et al. 1986; Davies and Von Blanckenburg 1995; Stern 2004; Ferrari 2004; Levander et al. 2014; Pilet et al. 2016). During this episode, a common paradigm is that the subducted materials—oceanic

Supplementary Information The online version contains supplementary material available at https://doi.org/10.1007/s11631-024-00755-6.

✉ Athokpam Krishnakanta Singh
aksingh_wihg@rediffmail.com

[1] Wadia Institute of Himalayan Geology, Dehradun 248001, India

[2] Department of Applied Geology, Dr. Harisingh Gour University, Sagar 470003, India

[3] Department of Geology, Banaras Hindu University, Varanasi 221005, India

[4] Nagaland University, Meriema, Kohima, Nagaland 797004, India

[5] CSIR-National Institute of Oceanography, Goa 403004, India

[6] Department of Earth Sciences, Indian Institute of Technology, Kanpur 208016, India

crust, sediments and oceanic mantle, contributed and influenced the formation of magmas and their composition (Leeman 2020). In a supra-subduction zone, the oceanic crust can be generated in three tectonic settings: island arc, back arc and fore arc. Another geologically recognized process in the development of a new subduction zone is the role played by subduction polarity reversal following arc-continent collision (Dewey 1976; Chemenda et al. 2001; Pysklywec 2001; Stern 2004; Faccenda et al. 2008; Plunder et al. 2020; Yang 2022). A subduction polarity reversal is a type of induced subduction initiation in which the subduction zone dip not only changes its direction but also the subducting and overriding plates exchange roles (Stern 2004; Yang 2022). Some of the examples and models of subduction polarity reversal are the Ontong Java Plateau-Solomon subduction system, Banda Arc, Andaman subduction system, Taiwan orogen and Kamchatka orogen (Yang 2022). During convergence, the arrival of a more buoyant continental or thickened oceanic lithosphere leads to the arrest of the original downgoing plate in the trench and is succeeded by the initiation of a new subduction zone within or behind the arc (Plunder et al. 2020). In most ophiolites, the affiliation of the mid-ocean ridge basalt (MORB-like) and island arc basalt (IAB) type mafic rocks subscribed to a distinct tectonic setting or a complex back-arc system (Dilek and Newcomb 2003; Dubois-Côté et al. 2005; Whattam and Stern 2011; Dai et al. 2012, 2013; Dilek and Furnes 2011; Furnes et al. 2012). The geological history and its general tectonic model are recreated using a variable proxy in conjunction with ophiolite stratigraphy (Dilek and Furnes 2011; Parlak et al. 2019; Bandyopadhyay et al. 2021). However, the geochemical signatures observed in the ophiolite of the eastern Indian plate margin are too diverse to be explained by a single tectonic setting.

Geochemical signatures of the mafic and ultramafic rocks of the Nagaland-Manipur Ophiolite (NMO) represent a more diverse tectonic signature of mid-oceanic ridge (MOR), supra-subduction zone (SSZ) and plume-related activity (Singh 2009, 2013; Ningthoujam et al. 2012; Khogenkumar et al. 2016, 2021; Singh et al. 2017a; Kingson et al. 2019; Ao and Satyanarayanan 2022; Chaubey et al. 2022). On the other hand, the genesis of the ANO mafic volcanic rocks (basalt, gabbro, metabasalt) have been subscribed to typical back-arc setting, island-arc, plume and N-MORB setting (Jafri et al. 1990; Srivastava et al. 2004; Pal 2011; Jafri and Sheikh 2013; Saha et al. 2019; Akhtar et al. 2021). However, recent studies by Plunder et al. (2020) and Bandyopadhyay et al. (2021) have proposed a possibility for subduction polarity reversal for the exposed back-arc setting rock in the Andaman-Nicobar ophiolite. It is widely assumed that the ophiolites of the eastern Indian plate (NMO, ANO), presently aligned in north to south position, are of the same forearc system and formed at the same subduction zone (Liu et al. 2016). This comes in support of the southward younging of the ophiolites of the eastern Indian plate (Advokaat et al. 2018; Khogenkumar et al. 2021) and the conceptual southward migration of the triple junction during polarity reversal (Advokaat et al. 2018; Plunder et al. 2020; Bandyopadhyay et al. 2021). It is also suggested that possible subduction polarity reversal records might be found in NMO (Advokaat et al. 2018). This idea is favored by the presence of MORB-like-arc geochemical signatures in the mafic rocks of the NMO. To ascertain the possible connection of subduction polarity reversal along the eastern Indian Plate margin, we re-evaluate the geochemical, mineralogical and geochronological characteristics of the MORB-like mafic rocks between NMO and ANO. In this paper, we present new geochemical data on NMO along with published data on NMO and ANO to explore and explain the possible tectonic scenario in relation to the regional plate kinematic evolution before the formation of ophiolites of NMO and ANO.

2 Regional geology

The Tethyan ophiolites exposed in the Alpine-Himalayan orogenic system are highly diverse in terms of their structural and petrological features and emplacement mechanisms (Nicolas et al. 1981; Allégre et al. 1984; Girardeau et al. 1985a; Girardeau et al. 1985b; Dilek and Newcomb 2003; Dilek and Furnes 2009). The Indus-Tsangpo suture zone (ITSZ) is one such suture zone, which represents the remnants of the Neotethyan oceanic lithosphere and marks the boundary between the Tethyan Himalaya of the Indian plate to the south and the Eurasian plate to the North (Fig. 1a, b). The Tethyan ophiolite suite of rocks of the ITSZ turn sharply southwestward at the eastern Himalayan syntaxis, being offset northward by the Sagaing Fault (Gururajan and Choudhuri 2003; Dutt et al. 2021a, b; Singh et al. 2022a). The 2000-km-long ITSZ that extends from east to west marks the collision of the Indian and Eurasian plates, where the Neotethyan ophiolite complexes are obducted and preserved along the suture (Tapponnier et al. 1981; Allégre et al. 1984). As the ITSZ extends southward, it encounters the NMO (Fig. 1c), which is a 200 km long, dismembered and tectonized suite of ophiolites trending NNE, formed in response to the collision of the Indian and Burmese plates. This ophiolite suite of rocks is represented by pelagic oceanic sediments, basalts (massive and Pillow), plagiogranites, cumulate gabbro and a suite of variously serpentinized to fresh ultramafic associations of dunite, harzburgite, lherzolite, wherlite and pyroxenites (Acharyya 1986; Venkatramana et al. 1986; Sengupta et al. 1990; Singh 2013; Ningthoujam et al. 2012; Singh et al. 2017a, b; Ghosh et al. 2018; Khogenkumar et al. 2016, 2021). The northern section of the NMO, referred to as the

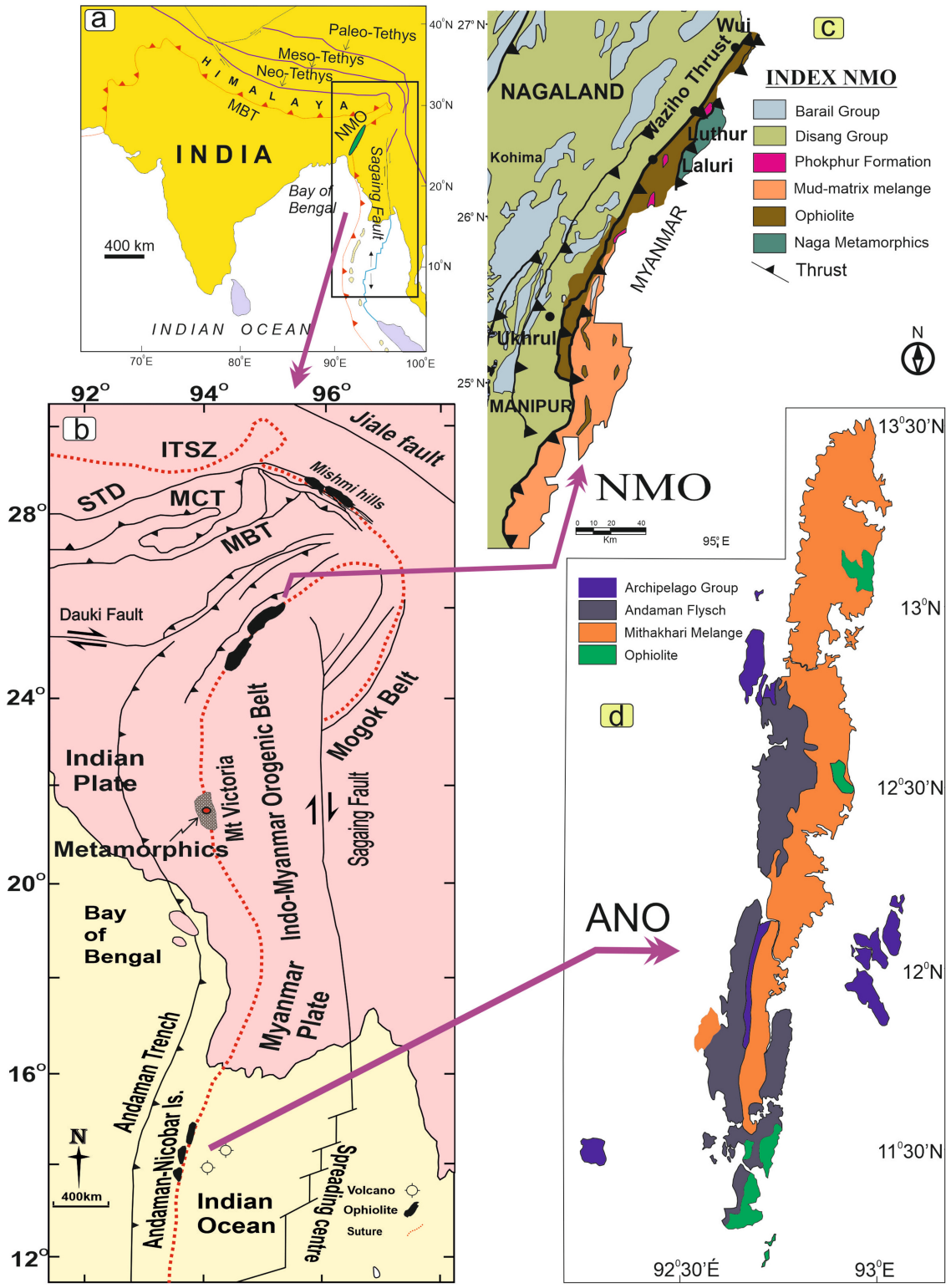

Fig. 1 (a&b) Global geologic map of northeast India and neighboring Myanmar (modified after Westerweel et al., 2019; Licht et al., 2019). (c) Geological map of Nagaland and Manipur, Northeast India (modified after Ningthoujam et al 2012; Agarwal and Ghose 1986; Directorate of Geology and Mining, Nagaland 2009). (d) Geological map of Andaman Nicobar islands (modified after Pal 2011). ITSZ- Indus-Tsangpo Suture Zone, MBT- Main Boundary Thrust, MCT- Main Central Thrust, STD- South Tibet Detachment

Nagaland ophiolite complex (NOC), exposed a majority of the volcanics of NMO along with ultramafic and pelagic sediments compared to the southern section, referred to as the Manipur ophiolite complex (MOC) (Singh et al. 2008, 2022a; Ningthoujam et al. 2012; Singh 2013; Ao and Bhowmik 2014; Khogenkumar et al. 2016, 2021; Bhowmik and Ao 2016; Kingson et al. 2019) where ultramafic exposure prevails. The NMO has an east-dipping thrust contact with the underlying Upper Cretaceous-Upper Eocene flysch-like sediments of the Disang and Barail formations exposed in the west and overthrusted from the east by metamorphic rocks of quartz mica-schist, garnet mica-schist, quartzite and granitic gneiss (Brunnschweiler 1966). Mafic intrusives are directly overlain in places by basalts and volcanic breccias that are intercalated with and covered by argillaceous and flyschoid sediments. Mafic volcanic rocks and radiolarian chert are closely associated and interbedded, occasionally with carbonates. Well-preserved basaltic flows exhibiting pillow structures are also observed (Singh et al. 2008; Khogenkumar et al. 2016). In some areas, a sharp contact between the ultramafic and chert is observed. The NMO podiform chromitites are predominantly exposed in the southern part, associated with peridotites (Ghose and Shrivastava 1986; Singh et al. 2013; Pal et al. 2014; Zaccarini et al. 2016; Maibam et al. 2017; Premi et al. 2022 2023). Massive chromitite is the most abundant while the nodular type is the least abundant in the study area (Singh et al. 2013; Chaubey et al. 2024). Minor metadolerite, metabasite, plagiogranite and late felsic rocks associated with Cu–Mo sulfide mineralization are also present in the NMO (Ghose et al. 2010).

The subduction zone of Andaman and Nicobar Islands is one of the few accretionary convergent margins where all the important components of a convergent margin are exposed, including a trench, an outer arc accretionary prism, a fore-arc, a volcanic arc and a back-arc basin (Fig. 1d). The geology of the Andaman Nicobar Islands consists of the Cretaceous ophiolite group (Andaman–Nicobar Ophiolite), Eocene Mithakhari group of sediments, Oligocene Andaman Flysch group and Archipelago group of Mio-Pliocene (Oldham 1885; Haldar 1985; Chakraborty and Pal 2001; Bandopadhyay 2005; Pal et al. 2003; Ghosh et al. 2013). The Mithakhari, Andaman Flysch and Archipelago groups comprise and represent sediments and deposits formed in the trenches, deep-sea fans and shallow marine shelves, respectively (Bandopadhyay 2012; Ghosh et al. 2018). The Andaman-Nicobar Ophiolite (ANO) consists of metamorphic rocks, mélange and ophiolite rocks (Haldar 1985; Ray et al. 1988; Roy 1992; Akhtar et al. 2022). The ophiolite rocks of ANO are comprised of harzburgites, ultramafic cumulates (dunites, wherlites, pyroxenites), cumulate gabbro and plagiogranite, massive and pillow basalts and pelagic sediments (Saha et al. 2010; Pal et al. 2003; Akhtar et al. 2021). The ANO is dismembered and forms the basement overlain by the Mithakhari group (Akhtar et al. 2021).

3 Field observations and petrography

Geological investigation, in general, was carried out in the northern section of NMO, i.e., NOC, which is a mountainous area, with the outcrop exposed at an altitude of > 1000 m. The study area is highly faulted, with the strata dipping mostly toward the NE direction. The collected samples are mostly gray to light green in color in both the massive basalt (Fig. 2a, b) and pillow basalt (Fig. 2c, d). The massive basalt exposure is prominent and is traversed by large-scale calcite veins in some sections ranging in width from 2 to 15 inches (Fig. 2b). Contact of massive basalt with agglomeratic basalt and pillow basalt is also encountered (Fig. 2b, c). The pillow basalt exposed is in continuity with the massive basalt. The pillow basalt is round to elliptical in shape with chilled margins, which is a characteristic of the eruptive nature of basalt in submarine conditions (Fig. 2d).

The general micro-petrographic studies of mafic samples from NMO do not reveal any remarkable mineralogical or micro-textural differences among the studied samples; henceforth, we will describe them as a single unit of rock, highlighting only the significant petrographic discrepancy when necessary. The primary minerals identified in the studied volcanic rocks of NMO are plagioclase and clinopyroxene with calcite and chlorite secondary minerals. They exhibit intersertal, variolitic and intergranular textures (Fig. 3a, b). A few samples of basalt also exhibit poikilitic and glomeroporphyritic textures where clinopyroxene and plagioclase crystals are embedded in a fine-grained groundmass of small microlites of plagioclase (hyalopilitic texture) and oxide minerals (Fig. 3c, d, f). This is a characteristic of crystal consolidation during magma ascent. Quartz is also present as veins in the basalt (Fig. 3d) along with chlorite mineral, which is an alteration product of pyroxene (Fig. 3e). In some samples, phenocrysts of plagioclase are partially or completely included in the inclusion of pyroxene (Fig. 3e). Variable degrees of alteration in the groundmass are observed in the basalt samples. Based on the petrographic data, samples were selected for whole rock geochemistry (major and trace elements) and mineral chemistry.

4 Ages through space and time

The first geochronological study on the NMO mafic rocks was attempted by Sarkar et al. using K–Ar isotopic age in a basalt rock and yielded 148 ± 4 Ma (1996). This was followed by the study of faunal assemblages in pelagic limestones of the NMO, which assigned it to the Late Cretaceous

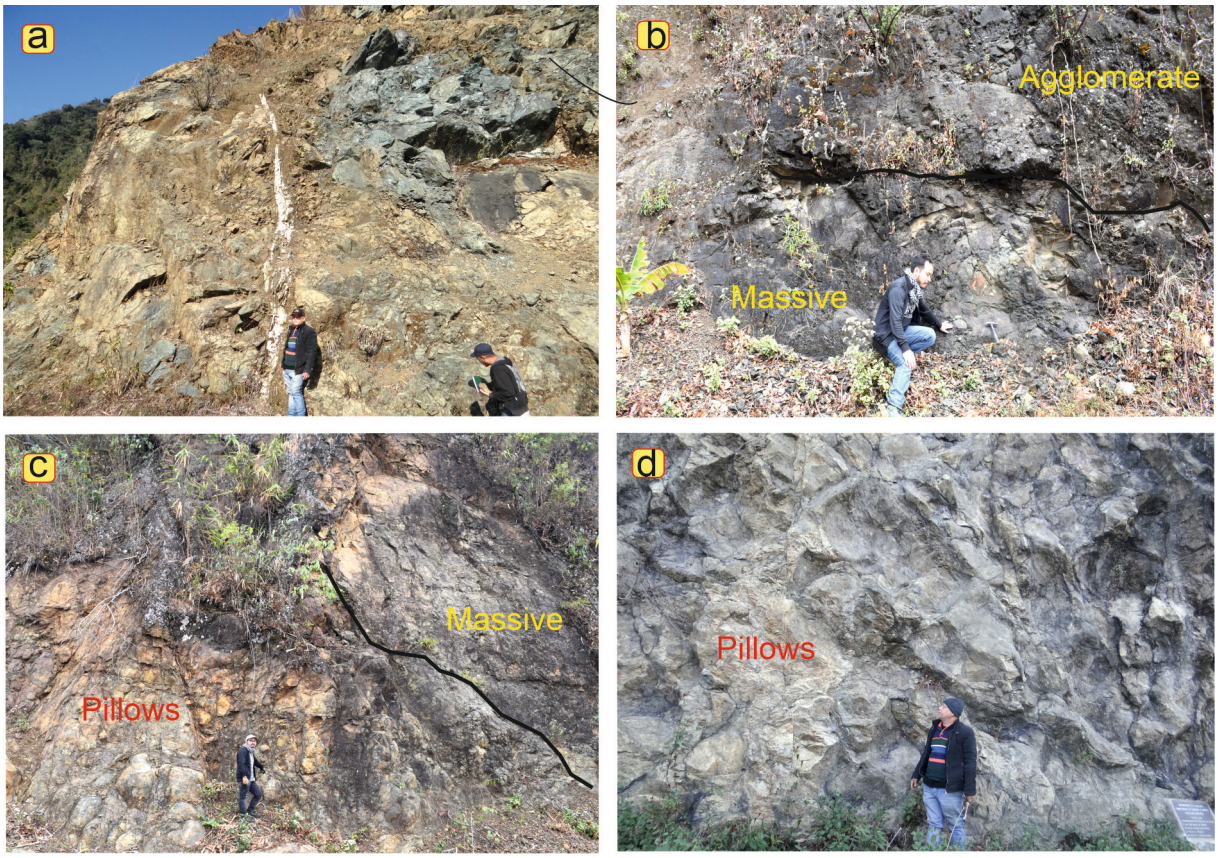

Fig. 2 Field photographs of typical outcrops of Nagaland Manipur Ophiolite, Northeast India (a) Massive basalt intruded by large calcite vein (b) Contact between Massive basalt and Agglomertic basalt (c) Contact between Pillow basalt and Massive basalt (d) Pillow basalt outcrop

(Chungkham and Jafar 1998). Another study proposed an Upper Jurassic age concordant with 148 Ma (K–Ar) from radiolarian-bearing chert (Baxter et al. 2011). However, most relative ages fall within the Cretaceous to Paleocene (Acharyya 1986; Chungkham and Jafar 1998). Recently, Guruaribam et al. (2022) and Singh et al. (2022b) suggested that the carbonate rocks from the NMO might have been formed in a neritic to bathyal palaeo-environment during the Santonian-Maastrichtian age.

Geochronological studies through zircon U–Pb analysis from plagiogranite (Singh et al. 2017a) and gabbro (Aitchison et al. 2019) yielded ages between 118.8 ± 1.2 and 116.63 ± 0.30 Ma for NMO formation, which is different from the earlier reported K–Ar isotopic age of 148 ± 4 Ma by Sarkar et al. (1996). The age range of 118.8 ± 1.2 to 116.63 ± 0.30 Ma, reported by Singh et al. (2017a) and Aitchison et al. (2019), has been attributed to the subduction of the Neotethyan plate in a SSZ setting, whereas the tectonic environment corresponding to the age of 148 Ma, as reported by Sarkar et al. (1996) and Baxter et al. (2011), remains undefined.

Along the eastern plate of Indian ophiolite, the ANO has the youngest ophiolite crust formation with ages between 98 and 93 Ma (Pedersen et al. 2010; Sarma et al. 2010; Bhattacharya et al. 2020). Another study in the metamorphic sole by the Ar/Ar method obtained ages of 106.4 ± 2.1 and 105.3 ± 1.6 Ma (Plunder et al. 2020). This supports the zircon U–Pb study on gabbro, which obtained variable ages of 105 and 98 Ma (Ray et al. 2015; Bandyopadhyay et al. 2021). According to this, the older 105 Ma age represents the magmatism or melting of the pre-existing gabbroic crust, while the youngest date, 98 Ma, represents the emplacement of gabbro in ANO. Existing geochronology data confirm that ophiolites along the eastern Indian plate, including NMO, were formed at different time scales. For NMO, a gap of ~ 31 Ma between the dated ages of 117 and 148 Ma make its interpretation as having a single magmatic origin improbable.

5 Analytical techniques

Petrological and geochemical data from NMO and ANO were used to investigate the MORB-like mafic rocks of the eastern margin of Indian ophiolite. Although the mafic volcanic samples of NMO were collected and analyzed

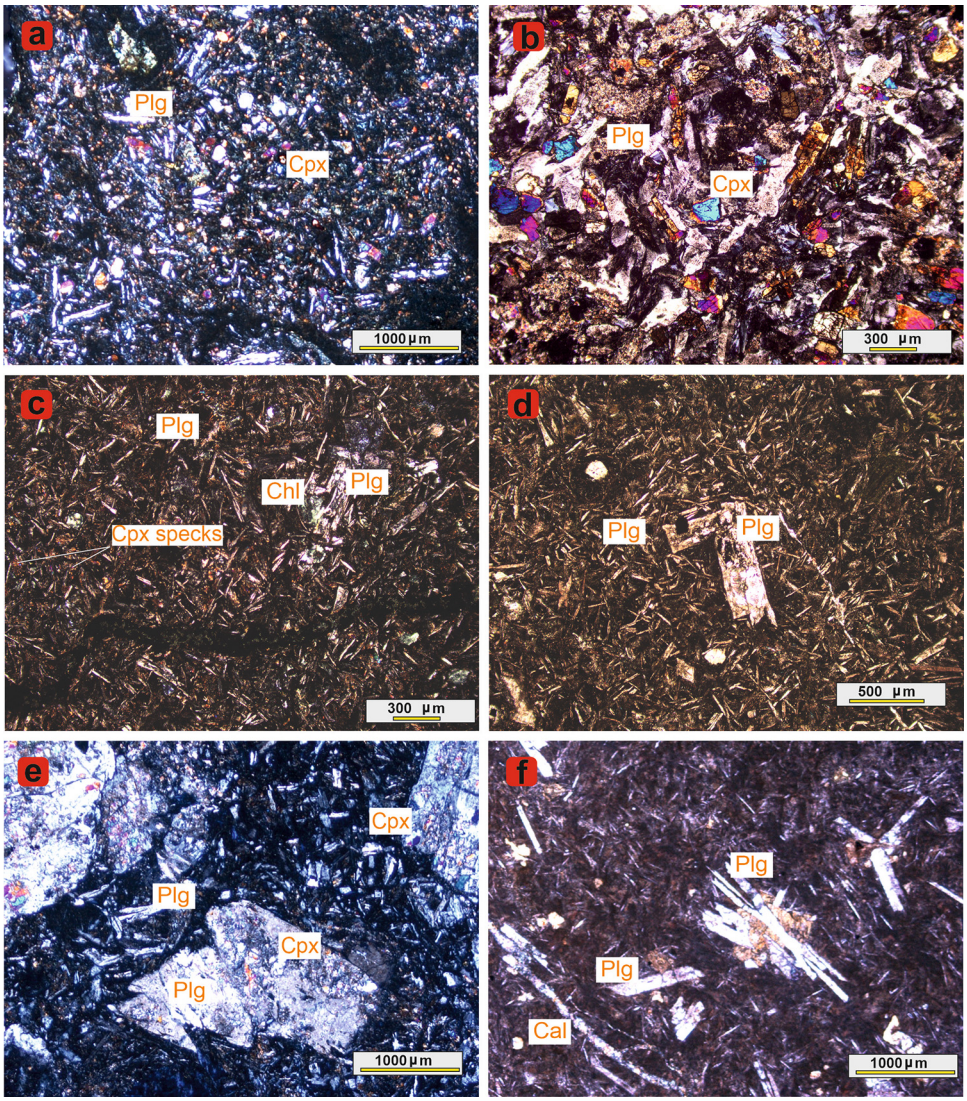

Fig. 3 Photomicrographs of Basalt from Nagaland Manipur Ophiolite. (a, b) Granular pyroxene (Cpx) and elongate plagioclase (Plg) showing intergranular texture. (c) Intersertal texture and Plagioclase (Plg) laths streaking out from a central point showing variolitic texture. (d, e) Exhibit poikilitic texture of plagioclase (Plg) crystals with inclusion of clinopyroxene (Cpx), and Calcite (Cal). (f) Glomeroporphyritic cluster of clinopyroxene (Cpx) and plagioclase (Plg) crystals in the fine-grained plagioclase and opaque

after several expeditions, the samples/data sources for mafic samples of ANO were compiled from previously published papers. The samples and data sources from NMO and ANO were selected based on their geochemical characteristics, in which they possess characteristics of both MORB and SSZ origin. Samples with datasets of both whole rock geochemistry and mineral chemistry were selected from ANO for this study.

Mineral analysis of the polished thin-section samples was carried out on a CAMECA Sx Five electron probe micro-analyzer at the Department of Geology, Banaras Hindu University, Varanasi. Analytical conditions were 15 kv accelerating voltage and 20 nA sample current with a 5-µm beam diameter. Instrument calibration was carried out using standard natural material, and replicated analyses of individual points produced an analytical error of $< 2\%$. Only clinopyroxene data are presented here and are used as discriminants of tectonic settings. The mineral chemistry data of clinopyroxene are presented in Table 1.

Fresh samples of basalt were cleared of weathered surfaces and veins prior to being crushed in an agate carbide ring grinder for subsequent major and trace element analysis. The major oxides and selected trace elements were analyzed at the Wadia Institute of Himalayan Geology (WIHG), Dehradun, using x-ray fluorescence (XRF; Bruker Tiger S-8) on pressed-powder pellets. Powder samples of about 0.5 g were heated at 1000 °C in a separate aliquot for 5 h to determine the loss on ignition (LOI) of each representative sample. The analytical precision for major oxides is commonly $\pm 2\%$–3% and $\pm 5\%$–6% for trace elements. For some trace elements and rare earth elements (REE), the powdered samples were digested using the open rock digestion method and were analyzed using an inductively coupled plasma-mass spectrometer (ICP-MS; PerkinElmer SCIEX ELAN DRC-e) at

Table 1 Compositions of representative clinopyroxene of basalt from Nagaland Manipur ophiolites, Northeast India

Sample No.	AKI 43							AKI 38		WAZPB-1								
Mineral	7/1	9/1	14/1	16/1	19/1	28/1	34/1	48/1	49/1	6/1	8/1	9/1	74/1	76/1	77/1	79/1	80/1	81/1
SiO_2	51.52	50.84	52.05	50.95	51.12	50.12	51.66	50.43	49.88	51.64	51.96	51.03	51.65	51.36	51.21	50.93	50.41	50.59
TiO_2	0.19	0.23	0.28	0.25	0.27	0.44	0.27	0.43	0.41	0.34	0.31	0.47	0.63	0.22	0.41	0.24	0.27	0.63
Al_2O_3	3.13	2.91	2.99	2.79	2.90	3.06	2.31	3.45	3.62	2.78	2.88	3.37	3.44	2.83	3.49	3.35	3.59	3.81
Cr_2O_3	0.42	0.62	0.44	0.34	0.34	0.10	0.23	0.59	1.14	0.77	0.53	1.11	0.69	0.79	0.76	0.71	0.89	1.00
Fe_2O_3	1.75	4.60	2.89	3.81	3.78	4.77	3.08	2.13	2.97	1.04	1.71	1.44	0.71	1.14	0.33	1.47	2.10	0.89
FeO	2.61	0.22	3.56	0.90	1.48	1.81	1.94	4.50	3.40	5.79	4.66	5.01	6.44	5.01	5.6	4.71	4.16	5.84
MnO	0.05	0.18	0.26	0.18	0.02	0.23	0.25	0.13	0.26	0.20	0.09	0.00	0.24	0.00	0.00	0.00	0.00	0.00
MgO	16.05	16.71	18.50	16.18	16.34	14.90	15.78	17.1	17.23	18.02	17.64	16.95	16.64	17.29	17.51	16.76	16.85	17.12
CaO	23.16	23.53	19.24	23.51	23.12	23.76	23.96	19.23	19.2	18.02	19.6	19.71	19.51	19.44	18.63	19.99	19.83	18.56
Na_2O	0.16	0.19	0.22	0.22	0.21	0.28	0.20	0.20	0.22	0.18	0.24	0.21	0.20	0.19	0.20	0.20	0.20	0.20
K_2O	0.03	0.00	0.01	0.02	0.04	0.00	0.03	0.01	0.01	0.01	0.00	0.00	0.02	0.00	0.00	0.00	0.00	0.00
Totals	99.07	100.03	100.44	99.15	99.63	99.47	99.71	98.19	98.34	98.78	99.62	99.29	100.17	98.27	98.14	98.36	98.3	98.64
Oxygens	6	6	6	6	6	6	6	6	6	6	6	6	6	6	6	6	6	6
Si	1.90	1.86	1.89	1.88	1.88	1.86	1.90	1.88	1.86	1.91	1.91	1.89	1.90	1.91	1.90	1.90	1.88	1.88
Ti	0.01	0.01	0.01	0.01	0.01	0.01	0.01	0.01	0.01	0.01	0.01	0.01	0.02	0.01	0.01	0.01	0.01	0.02
Al	0.14	0.13	0.13	0.12	0.13	0.13	0.10	0.15	0.16	0.12	0.13	0.15	0.15	0.12	0.15	0.15	0.16	0.17
Cr	0.01	0.02	0.01	0.01	0.01	0.00	0.01	0.02	0.03	0.02	0.02	0.03	0.02	0.02	0.02	0.02	0.03	0.03
Fe_3	0.05	0.13	0.08	0.11	0.11	0.13	0.09	0.06	0.08	0.03	0.05	0.04	0.02	0.03	0.01	0.04	0.06	0.03
Fe_2	0.08	0.01	0.11	0.03	0.05	0.06	0.06	0.14	0.11	0.18	0.14	0.16	0.20	0.16	0.17	0.15	0.13	0.18
Mn	0.00	0.01	0.01	0.01	0.00	0.01	0.01	0.00	0.01	0.01	0.00	0.00	0.01	0.00	0.00	0.00	0.00	0.00
Mg	0.88	0.91	1.00	0.89	0.90	0.83	0.87	0.95	0.96	0.99	0.97	0.93	0.91	0.96	0.97	0.93	0.94	0.95
Ca	0.92	0.92	0.75	0.93	0.91	0.95	0.95	0.77	0.77	0.71	0.77	0.78	0.77	0.78	0.74	0.80	0.79	0.74
Na	0.01	0.01	0.02	0.02	0.02	0.02	0.01	0.01	0.02	0.01	0.02	0.02	0.01	0.01	0.01	0.01	0.01	0.01
K	0.00	0.00	0.00	0.00	0.00	0.00	0.00	0.00	0.00	0.00	0.00	0.00	0.001	0.00	0.00	0.00	0.00	0.00
Fs	4.27	10.26	7.11	8.76	8.74	10.98	7.19	5.54	7.54	2.80	4.39	3.78	1.93	3.01	0.90	3.85	5.42	2.43
En	39.18	37.27	45.53	37.20	37.79	34.31	36.85	44.46	43.73	48.60	45.29	44.49	45.14	45.66	48.01	43.85	43.45	46.81
Wo	56.54	52.48	47.35	54.05	53.47	54.71	55.96	50.00	48.73	48.60	50.32	51.73	52.93	51.33	51.08	52.30	51.13	50.75

WIHG. The accuracy range of the rare earth elements is between 2% and 12%, while their precision varies from 1% to 8%. Whole rock, major, trace elements and rare earth elements are presented in Table 2.

6 Mineral chemistry

The pyroxene grains analyzed for mineral chemistry are anhedral and are classified as diopside ($Wo_{47.4–56.5}$, $En_{34.3–48.6}$, $Fs_{0.9–11}$) under the pyroxene classification of Morimoto et al. (1989, Fig. 4a). The composition of clinopyroxene in the basalts of NMO shows high Mg numbers varying between 82.1 wt% and 99.2 wt% with Al_2O_3 (2.31 wt%–3.81 wt%), TiO_2 (0.19 wt%–0.63 wt%) and Na_2O_3 (0.16 wt%–0.28 wt%) (Table 1). Although controlled by crystal chemical constraint, the chemistry of clinopyroxene is homogeneous and strongly represents the composition of magmas and the conditions from which they crystallize (Leterrier et al. 1982; Beccaluva et al. 1989). Therefore, the compositions of clinopyroxene were used to discriminate the affinity of basaltic magma and its tectonic setting in further discussion. In the Ti vs. (Na + Ca) covariation diagram of Leterrier et al. (1982), the clinopyroxene of the basalt plot in both the fields of alkaline and tholeiitic, with most points plotting in the tholeiitic field while the points from AKI 43 (except point 14/1) fall in the alkaline field (Fig. 4b), suggesting a different magma nature involved in the generation of these investigated mafic rocks.

7 Whole-rock geochemistry

Major and trace element data of the studied basalt samples are listed in Table 2. The basalt of NMO shows variable values of LOI 4.14 wt%–7.96 wt% with SiO_2 ranging between 45.46 wt%–52.97 wt%, Al_2O_3 9.13 wt%–14.99 wt%, Fe_2O_3 10.01 wt%–16.33 wt%, MgO 7.61 wt%–20.63 wt% and TiO_2 0.98 wt%–1.94 wt%. The TiO_2 concentrations with > 1 wt% (average 1.32 wt%) show more affinity toward MORB (1.6 wt%; Hofmann 1988) than those of island arc basalt (0.64 wt%; Condie 1989). These analysed samples with Zr/TiO_2 44.96–67.95 and Nb/Y < 0.50 can be classified as andesite/basalt to subalkaline basalt and alkaline basalt, according to Winchester and Floyd (1977) (Table 2).

The samples of the NMO show a LREE pattern ranging from slightly depleted LREE [$(La/Yb)_N = 0.44–0.69$] to enriched LREE [$(La/Yb)_N = 1.00–2.45$] comparable to D-MORB and E-MORB type magmatism, respectively (Fig. 5a). The ∑REE concentration of the basalts from NMO ranges between 10.40 and 71.43 ppm with an average of 38.31 ppm (Table 2). The basalts do not show any remarkable Eu anomaly with Eu/Eu* values between 0.85 and 1.09. On the primitive mantle normalized trace element, all the samples show depletion in Ba and Nb with consistent enrichment of Th (below detection limit for some samples), U and Pb typical of a subduction setting (Fig. 5b). The high LOI content and Pb enrichment observed in the samples might be the result of alteration. However, consistent enrichment of U observed in the samples is likely to have originated from a magmatic process. Since possible effects of alteration are evident from mineral chemistry as well as the whole-rock geochemistry, we relied upon high-field strength elements and TiO_2, which are more resistant to alteration for further geochemical interpretation. A comparative REE pattern of typical SSZ, MORB and OIB from NMO is provided in Fig. 5c. Here, SSZ samples (from literature data; Singh et al. 201) are distinguishable from MORB data, exhibiting depleted LREE [$(La/Yb)_N$ 0.458] (avg.), low TiO_2 (0.675, avg.), and a total REE of 17.445 (avg.). In contrast, MORB samples display a flat REE pattern [$(La/Yb)_N = 0.978$] (avg.) with higher total REE (35.14, avg.) and TiO_2 content (1.09, avg.) (Supplementary Tables 3, 4, 5). The studied samples with [$(La/Yb)_N = 1.1$] (avg.), total REE 38.31 (avg.) and TiO_2 1.27 (avg.) is comparable with MORB rather than SSZ REE pattern. In Fig. 5c, the OIB REE pattern can be distinguished by its highly fractionated LREE [$(La/Yb)_N = 8.001$] (avg.) and a significantly higher total REE 121.70 (avg.) and TiO_2 2.02 (avg.) (Supplementary Tables 3, 4, 5).

The dataset published by Akhtar et al. (2022) and Bandyopadhyay et al. (2021) from ANO contributes its mafic (basalt and metabasic) petrogenesis in a back-arc basin setting. The geochemical of this ophiolite suite is characterized by a high LOI of 0.9 wt%–9.73 wt% with TiO_2 ranging between 0.48 wt%–1.57 wt% and MgO between 3.84 wt%–8.79 wt% (Supplementary Table 1). The REE pattern with $(La/Yb)_N = 0.68–2.05$ (7.09 for one sample) and total REE between 31.76–87.70 ppm exhibits slight depletion of LREE to flat LREE (except for one highly fractionated LREE) relative to MREE (Fig. 5a). The samples show weak to no Eu anomaly ranging between 0.69–1. The primitive mantle normalized trace elemental pattern shows enrichment in Rb, Pb, Ba, K and Th and depletion in Nb and Ti (Fig. 5b). The pyroxene chemistry with Cr_2O_3 0.11 wt%–0.9 wt%, Na_2O_3 0.28 wt%–0.7 wt%, Al_2O_3 2.56 wt%–6.49 wt%, TiO_2 0.49 wt%–1.9 wt% and CaO 16.69 wt%–20.72 wt% classified it as diopside in the pyroxene classification of Morimoto et al. 1989 (Supplementary Table 2).

8 Discussion

8.1 Source characterization and genetic relationship

The Nagaland-Manipur ophiolite represented by ultramafic, mafic and its associated pelagic sediments are remains of

Table 2 Major, trace element and REE composition of mafic samples from the Nagaland ophiolite complex, Northeast India

Sample	AKI38	AKI39	AKI19H	AKI24	AMI16	AI17	AKI36	AI20	AI22	AI28	NKK1	NKK2	NKK4	NKK12	NKK14
SiO_2	49.07	48.88	48.74	45.46	48.99	47.37	46.31	47.24	52.34	49.06	47.47	49.50	49.33	47.21	47.63
TiO_2	1.30	1.25	1.22	1.94	0.89	1.27	1.32	1.56	1.14	1.34	1.14	1.13	1.23	1.14	1.24
Al_2O_3	12.98	13.50	11.21	12.99	13.25	11.58	13.95	15.53	13.20	12.61	14.98	12.89	13.12	15.00	13.15
Fe_2O_3	11.56	10.97	11.96	16.33	10.70	11.45	10.51	9.47	10.01	12.90	13.96	10.94	11.02	11.97	11.97
MgO	11.04	11.18	11.32	12.26	10.22	10.31	7.69	9.50	7.61	11.57	12.44	11.12	11.25	4.86	9.63
CaO	10.31	10.83	12.69	8.15	9.57	8.70	15.82	6.84	10.44	9.63	5.91	13.06	13.29	18.48	12.69
Na_2O	3.30	3.07	2.33	2.49	2.39	2.52	2.72	3.67	4.20	2.56	2.35	1.08	0.43	0.96	3.09
MnO	0.21	0.17	0.21	0.20	0.20	0.17	0.15	0.17	0.14	0.21	0.18	0.18	0.19	0.22	0.23
K_2O	0.15	0.05	0.22	0.03	0.47	0.03	1.36	0.16	0.82	0.03	1.53	0.04	0.07	0.05	0.29
P_2O_5	0.09	0.09	0.09	0.15	0.09	0.09	0.16	0.16	0.09	0.08	0.03	0.05	0.06	0.11	0.08
LOI	5.43	5.19	4.49	5.27	3.00	5.81	6.17	5.24	4.7	4.97	4.14	5.14	6.12	6.21	4.98
Total	96.38	96.65	95.6	95.41	96.77	99.30	93.24	99.54	94.91	94.89	95.97	95.21	93.96	93.82	95.86
Trace elements															
Cr	404	312	154	252	164	304	332	211	375	366	532	314	374	328	566
V	291	307	312	377	297	290	255	217	254	329	287	323	367	368	337
Sc	42	41	50	46	49	33	38	27	34	41	53	44	48	48	42
Co	49	52	51	51	58	51	52	37	50	50	71	59	63	79	53
Ni	176	135	76	141	76	134	106	104	131	145	195	117	116	97	151
Cu	96	104	75	92	47	77	66	126	74	103	185	86	88	33	78
Zn	85	75	89	122	72	79	74	96	58	86	118	86	90	96	89
Ga	14.87	15.56	15.35	20.77	14	13	14.28	14	8.68	12.87	16.99	14.2	15.03	19.29	13.42
Pb	1.7	2.1	1.7	0.75	3	6	3.8	1	1.6	1	1.7	6.3	5.1	28.1	2.4
Th	0.81	0.56	1.14	1.03	1.0	2	1.86	1	0.05	0.07	1.41	0	0	0	0
U	0.41	0.29	0.4	0.34	0.4	0.4	1	0.8	0.93	0.57	0	0	0	0	0
Rb	0.88	1	2	0.31	6	1.0	21	2	14	1	37	0	1	1	6
Sr	96	159	305	118	155	65	317	143	239	154	43	228	42	23	114
Y	25	25	25	39	17	28	25	26	25	30	33	26	27	24	27
Zr	73	68	63	128	39	75	85	126	65	70	59	62	70	60	67
Nb	2.9	2.6	3	4.9	2	4	8.3	3	3.7	2.4	2.3	0	0	0	2.6
Ba	36	28	56	36	46	34	115	36	68	29	134	10	14	16	20
Rare earth elements															
La	5.61	4.84	6.12	6.36	2.724	2.717	9.71	2.758	0.79	1.62	1.83	1.89	1.76	1.65	2.62
Ce	14.91	12.88	15.18	17.58	7.551	6.578	21.57	6.586	2.61	6.00	5.26	5.97	6.01	5.36	7.17
Pr	1.98	1.80	2.15	2.60	1.266	1.051	3.11	0.865	0.41	0.90	0.98	1.28	1.19	1.07	1.30
Nd	9.20	8.46	9.76	12.47	6.041	4.977	13.52	4.264	2.09	4.80	5.14	6.68	6.49	5.86	6.81
Sm	2.88	2.63	2.97	3.95	1.988	1.675	3.74	1.318	0.70	1.73	1.99	2.53	2.48	2.29	2.41

Table 2 (continued)

Sample	AKI38	AKI39	AKI19H	AKI24	AMI16	AI17	AKI36	AI20	AI22	AI28	NKK1	NKK2	NKK4	NKK12	NKK14
Eu	0.93	0.87	1.06	1.40	0.805	0.587	1.32	0.482	0.23	0.61	0.81	0.96	0.91	0.85	0.87
Gd	3.83	3.40	3.94	5.20	2.523	2.3	4.72	1.525	0.87	2.14	2.65	3.36	3.34	3.07	3.23
Tb	0.71	0.61	0.73	0.94	0.47	0.451	0.80	0.272	0.15	0.41	0.52	0.64	0.65	0.60	0.62
Dy	4.64	4.21	4.84	5.94	3.126	2.861	5.10	1.71	1.00	2.78	3.52	4.31	4.31	4.13	4.25
Ho	1.04	0.93	1.09	1.28	0.668	0.661	1.11	0.373	0.22	0.60	0.81	1.00	0.96	0.94	0.96
Er	2.96	2.59	3.11	3.42	1.738	1.787	3.02	0.945	0.58	1.64	2.19	2.69	2.61	2.59	2.65
Tm	0.47	0.42	0.46	0.53	0.292	0.273	0.45	0.138	0.08	0.25	0.35	0.41	0.42	0.40	0.41
Yb	3.07	2.75	2.97	3.41	1.791	1.8	2.84	0.911	0.56	1.67	2.26	2.72	2.69	2.66	2.71
Lu	0.49	0.43	0.43	0.51	0.268	0.27	0.45	0.122	0.09	0.24	0.35	0.42	0.41	0.41	0.43
∑ REE	52.71	46.84	54.83	65.59	31.25	27.98	71.43	22.269	10.40	25.40	28.66	34.86	34.23	31.88	36.44

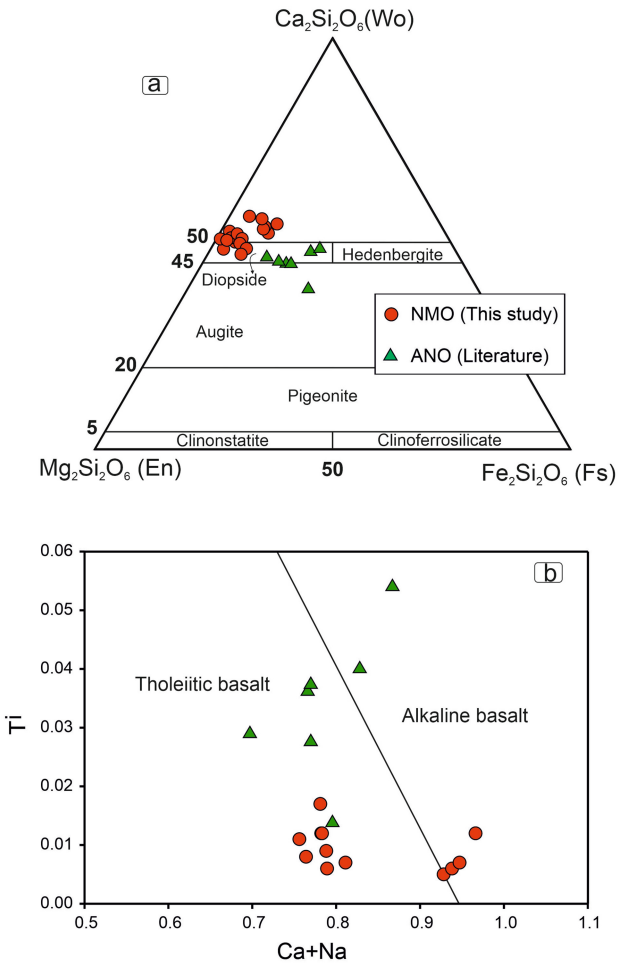

Fig. 4 (a) Mg-Fe-Ca pyroxene classification diagram of basalt from Nagaland Ophiolite complex after Morimoto et al.,1989. (b) Discrimination diagram of Ti vs Ca+Na based on clinopyroxene compositions of mafic (after Leterrier et al.1982)

Tethyan oceanic crust generated from a diverse tectonic setting (Ghose and Singh 1980; Acharyya 1986; Venkatramana et al. 1986; Sengupta et al 1989, 1990; Ningthoujam et al. 2012; Singh 2013; Khogenkumar et al 2016 2021; Singh et al. 2022a) (Supplementary Table 3, 4, 5). For a brief interval, the evolution of the NMO was debated between SSZ (Singh 2009, 2013, 2016; Ningthoujam et al 2012) and MORB setting (Khogenkumar et al 2016); however, this premise has been negated by the evolution of plume-related OIB, reported from NMO (Khogenkumar et al. 2016). The SSZ signature reported from both ultramafic and mafic of NMO represents a Tethyan oceanic plate subduction before its final obduction. The U/Pb radiometric studies conducted from zircons of plagiogranite (Singh et al. 2017a) and gabbro (Aitchison et al. 2019) indicate the subduction age of NMO at early cretaceous (118.8 ± 1.2 to 116.63 ± 0.30 Ma). Although the timing and evolution of MORB and OIB type of NMO have not been established, Khogenkumar et al.

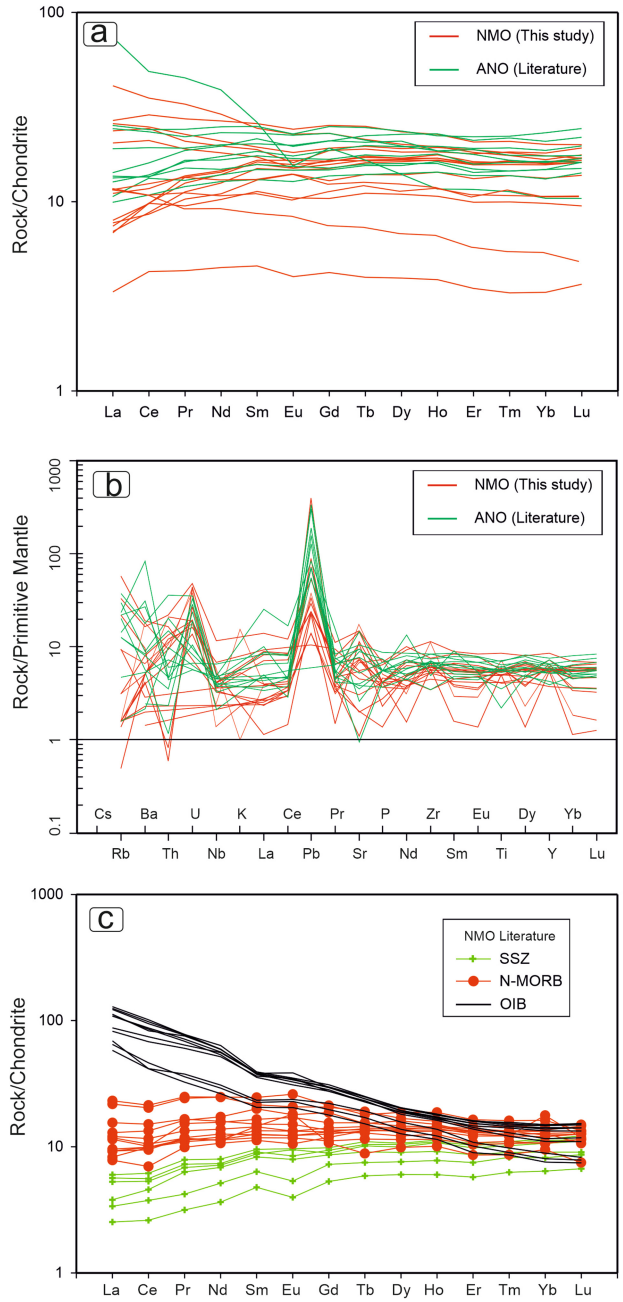

Fig. 5 (a) Chondrite normalized REE patterns of mafic from NMO and ANO showing flat to slightly enriched LREE compatible to MORB source. Normalization values are from Sun and McDonough, 1989. (b) Primitive mantle normalized trace elements diagrams of mafic from NMO and ANO. Normalization values are from Sun and McDonough, 1989. (C) Chondrite normalized REE patterns of published mafic rocks of SSZ, MORB, and OIB from NMO. The SSZ, MORB, and OIB data are from Singh et al., 2009, 2013, and 2016; Khogenkumar et al. 2016. Normalization values are from Sun and McDonough, 1989

(2016) suggested that the evolution of MORB and OIB might be related to the Indian-Australian plate rifting and occurred before its subduction during early cretaceous (118.8 ± 1.2 to 116.63 ± 0.30 Ma). It is also proposed that the MORB generation, which occurred during the India-Australian plate rifting, might be in proximity to OIB. Recently, a heterogeneous mantle source signature has been presented, which supports an extensional rift environment for its generation (Verencar et al. 2022; Imtisunep et al. 2022).

In the Andaman and Nicobar Islands, the Indian plate subducts toward the east below the SE Asian plate and exposed the ophiolites along the east coast of the North, Middle, South Andaman and Rutland Islands. Although limited data are available on the complete suite of the ANO, the basaltic rocks have been studied extensively. Over the years, the origin of the basaltic rocks has been attributed to N-MORB, Island arc and back-arc tectonic settings (Akhtar et al. 2021; Pal 2011; Saha et al. 2019; Jafri and Sheikh 2013; Jafri et al. 1990; Srivastava et al. 2004). However, the age and timing for the obduction of ANO are still controversial, with two notable independent schools of thought. One research group suggests that the formation of ANO could not be younger than ~ 95 Ma, as evident from the U–Pb dating of SSZ affinity plagiogranite zircon (Pederson et al. 2010; Sarma et al. 2010). The studies report a similarity in ANO age with Oman and Cyprus ophiolites and suggest the ANO to be an extension of the Late Cretaceous Tethyan suture zone ophiolite. The similarity in age of the Oman and Cyprus ophiolites and ANO seems best explained by a supra-subduction zone in which subduction initiation is followed by supra-subduction spreading (back arc) and explains the age relationship as well as the MORB-like basalt of ANO. However, Plunder et al. 2020 and Bandyopadhyay et al. 2021 suggest a relatively older age of about 106.4 ± 2.1 Ma and 105.3 ± 1.6 Ma for amphibolite rock using Ar/Ar method from the metamorphic sole of ANO. They argued that the back-arc affinity amphibole occurred because of the subduction of the back-arc plate that occurred southwest of the Woyla Arc and represented the initial subduction initiation before the maturation of the arc and the final collision of the Woyla Arc and SE Asian plate.

The studied basalt on the eastern margin of Indian ophiolite has high MgO (NMO average 10.84 wt%, ANO average 6.65 wt%), Cr (NMO average 784.3 ppm, ANO average 418.75 ppm) and Ni (NMO average 663.8 ppm, ANO average 374.16 ppm) content, indicating mantle-derived components. This is also supported by the geochemical signatures of MORB-like REE patterns and higher abundances of TiO_2 (NMO average 1.1 wt%, ANO average 1.20 wt%), in which the typical arc-derived source has $TiO_2 < 1$ wt% (Perfit et al 1980). In the Ti vs V plot, the studied samples of NMO and ANO have a Ti/V ratio > 20 and fall in the overlapping MORB and BABB fields along with the MORB samples in the literature data (Singh et al. 2016; Khogenkumar et al. 2016), signifying its affinity toward a mantle MORB source (Fig. 6a). Subsequently, the SSZ (literature data; Singh et al.

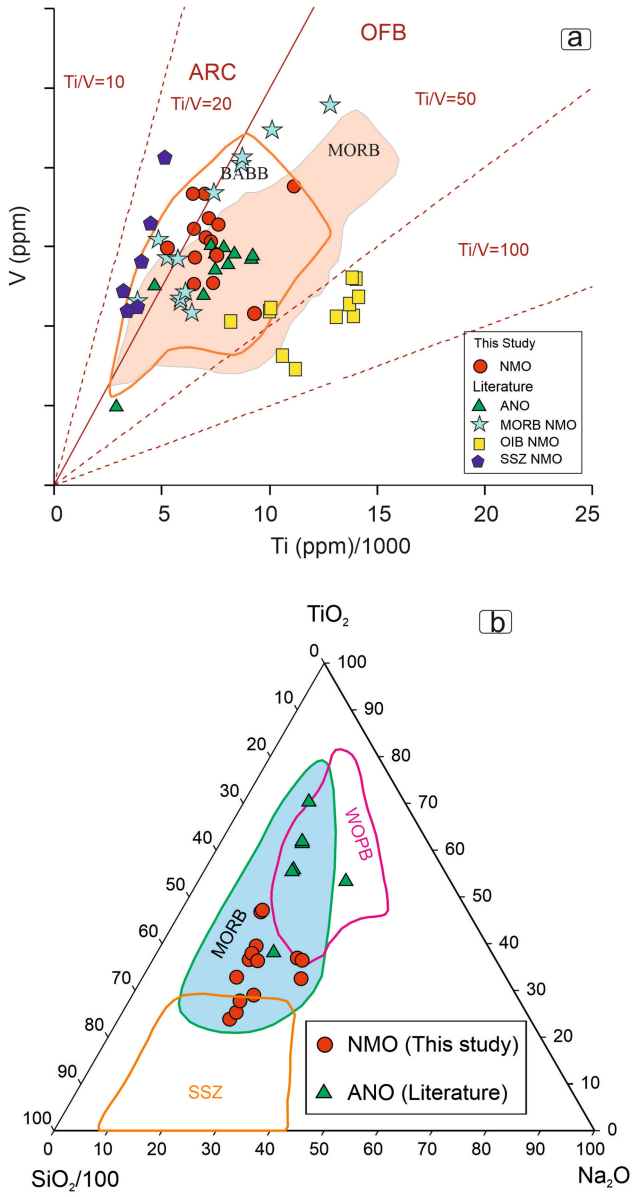

Fig. 6 (a) Ti vs V (Shervais, 1982) elemental plot of mafic from NMO and ANO. MORB = Mid Ocean Ridge Basalt, BABB = Back-arc Basin Basalt (from McLennan, 2001). (b) Tectonomagmatic plot of TiO2-SiO2/100-Na2O based on the clinopyroxene compositions of basalt from NMO and ANO after Beccaluva et al 1989

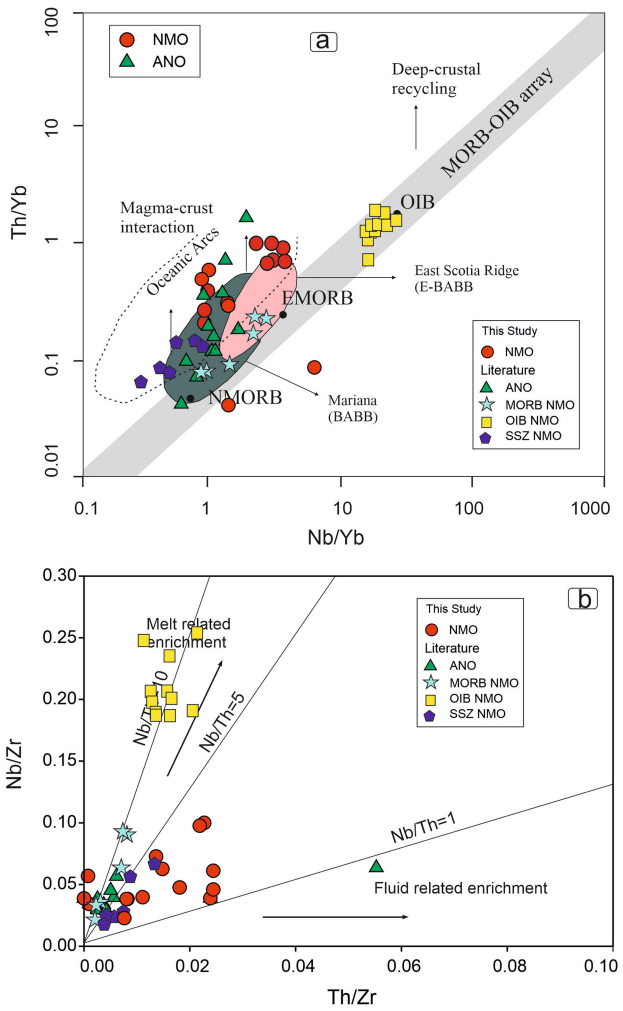

Fig. 7 (a) Th/Yb vs. Nb/Yb diagram modified after Pearce (2014), to investigate the crustal influence on mafic rocks of NMO and ANO. The oblique yellow field outlines the MORB-OIB array by Pearce (2008). The N-MORB, E-MORB, and OIB are from Sun and McDonough (1989). The compositions of Mariana Trough BABB from Pearce et al., 2005 and East Scotia Ridge E-BABB from Leat et al 2000. (b) Th/Zr vs Nb/Zr diagram showing the mafic samples in an array consistent with melt-related enrichment with slight input of fluid-related enrichment of mantle through subduction process for NMO and ANO samples

2016) with Ti/V < 20 falls in the arc field, while the OIB (literature data; Khogenkumar et al. 2016) falls in the field with higher Ti/V > 50. This MORB component is supported by the mineral chemistry of the clinopyroxene in which the discrimination diagram of SiO_2/100–TiO_2–Na_2O (Fig. 6b) reveals, in the studied samples and ANO samples, a close affinity with the clinopyroxenes of MORB. Therefore, it is likely that the studied mafic volcanic of these ophiolites could have their components from MORB-like asthenospheric sources.

In contrast, it is also observed that the mafic volcanics from the eastern Indian ophiolite (NMO and ANO) show high LILE (like Rb, Ba, and Th) abundances, negative Nb and positive Pb anomalies (Fig. 5b), which are characteristic of a typical island arc setting. This trend of slab component involvement is supported by Th/Yb vs Nb/Yb (Fig. 7a) in which the studied samples and ANO samples plot away from the mantle array and fall onto the mantle-crust interaction field along with SSZ samples (literature data; Singh et al. 2016). Meanwhile, the comparative samples of MORB and OIB from NMO fall in their respective field of mantle array with no crust involvement. However, the interaction of the

mantle and crust components in the studied samples also raises doubt about crustal contamination. Thus, its effect should be considered before discussing the magma source. The studied samples have MORB-type REE patterns along with relatively constant of SiO_2, V and TiO_2, which argues against crustal contamination. In addition, the La/Nb ratio of the studied samples also does not increase with increasing SiO_2 (Table 2), as it is known that the ratio of La/Nb increases when contaminated by continental crust (Rudnick 2005) and thus contradicts a significant crustal contamination. It is likely that this source might have been metasomatized by fluid or melt released from the subducting melt. Generally, the involvement of slab-derived fluids is credited to high Sr/Nd, while the injection of subducted sediments is attributed to high Th/Yb with low Sr/Nd (Davidson 1987). The studied samples have higher Sr/Nd ratios (NMO average 25.45; ANO average 19.37) than MORB (12.3, Sun and McDonough 1989), indicating the involvement of slab-derived fluids. In the elemental mobility of the Th/Zr and Nb/Zr ratio, the mantle source metasomatized by the slab-derived fluid is true for most of the studied samples and SSZ samples (literature; Singh et al. 2016) with Nb/Th values ranging between 1 and 5, while some of the studied samples, ANO samples, MORB and OIB show a trend toward melt-related enrichment components (Fig. 7b). In summary, although the studied samples from NMO and the literature data (Akhtar et al. 2022; Bandyopadhyay et al. 2021) of ANO samples exhibit similar geochemical signatures, they can be regarded as distinct entities compared to SSZ, MORB and OIB samples (Singh et al. 2016; Khogenkumar et al. 2016). The studied samples from NMO and the literature data of ANO trend toward a mantle source that interacted with crustal components, although less significantly than the SSZ source.

Earlier published studies have shown that the mafic basalts of NMO and ANO were generated mainly from spinel-bearing mantle sources (Bandyopadhyay et al. 2021; Imtisunep et al. 2022; Akhtar et al. 2022). Since the studied samples appear to be affected by either mantle heterogeneity or partial melting, the elemental plot of Cr versus Y (Fig. 8) is used to illustrate the possible mantle source and relative degrees of partial melting of the mafic volcanics of different studied ophiolites (Pearce 1983). As partial melting of the mantle increases, compatible Cr remains relatively unchanged, while Y concentrations in the melt become diluted and decrease. In accordance with the model for the incremental batch melting starting from a single source by Murton (1989), three possible mantle sources were considered. Figure 8 indicates that most of the samples from the studied ophiolites are compatible with about 15%–30% partial melting of undepleted MORB source S1. However, not all the samples of NMO and ANO are compatible with 15%–30% partial melting of Source

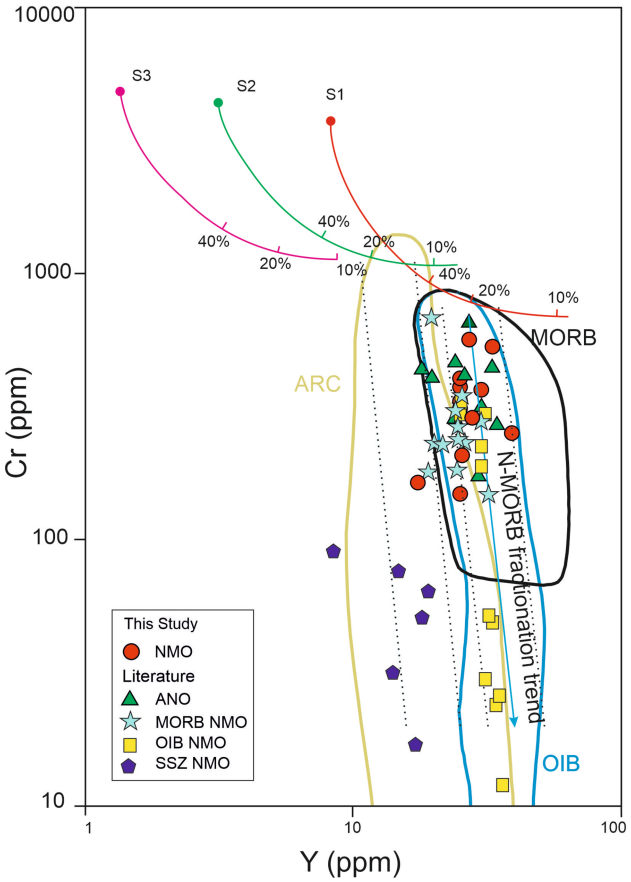

Fig. 8 Cr vs. Y diagram for mafic rocks of NMO and ANO modified after Pearce 1983. Mantle source compositions and melting path for incremental batch melting are from Murton 1989. S1- undepleted mMORB source; S2- residue after 20% MORB melt extraction from source S1; S3- residue after 12% melt extraction from source S2. Field of ARC, MORB and OIB from McLennan, 2001

S1. Some of the mafic samples (2 samples from ANO, 1 studied sample and 3 MORB samples from NMO), assuming they originated from mantle source S1, intersect the melting path above 40%—a rather excessive degree of partial melting, given that the rocks exhibit REE enrichment. Instead, these samples are more likely derived from approximately 15% partial melting of the M2 source. In contrast, the higher degrees of partial melting above the subducting slab caused the SSZ samples of the NMO to exhibit lower Y concentrations compared to the others and underwent 15%–30% partial melting of the M2 source. The OIB samples from NMO, following the fractionation trend, plot along the 20%–30% partial melting of mantle source S1, as Cr concentrations decrease in the melt because of partitioning into the crystallizing mafic phase. In summary, studied samples have been derived from 15% to 30% partial melting of a relatively undepleted MORB-type source 1% and 20% MORB melt extract residue (S2) and fall in the overlapping field of MORB and OIB.

8.2 Implication for the geodynamic evolution

The Neotethys ocean subducted beneath the Eurasian plate and shaped the formations that formed on the eastern boundary of the Indian plate from the early Cretaceous of NMO (~ 118 Ma; Singh et al. 2017a; Aitchison et al. 2019) till the Late Cretaceous of ANO (~ 95 Ma; Pedersen et al. 2010; Sarma et al. 2010). As examined above, the overall geochemical characteristics and mineralogical compositions of the mafic rocks on the eastern margin of Indian ophiolite are comparable and provide strong evidence of either a suprasubduction or within-plate setting, although complications exist for both. In the Ce/Nb–Th/Nb (Fig. 9) tectonic discrimination diagram, Th and Ce are used to discriminate between MORB and arc basalts, where Ce is elevated in arc basalts, relative to MORB. In Fig. 9, the studied samples, along with the literature data (Akhtar et al. 2022; Bandyopadhyay et al. 2021) of ANO, are scattered along a trend of increasing Th but primarily fall within the back-arc basin field, whereas the literature data (Singh et al. 2016; Khogenkumar et al. 2016) of MORB and OIB plot within the E-MORB field. Furthermore, the studied samples do not exhibit the same synchronous increase in Ce with Th as observed in the arc basalts (SSZ). The diverging vectors in the Ce/Nb-Th/Nb diagram suggest the possibility that the arc character may result from AFC, as supported by the sub-parallel trend of the studied samples with the AFC vector (rather than the arc trend).

A non-Th-based discrimination diagram lacks the arc indicator and complicates the volcanic arc setting, while within-plate settings require the process for Th enrichment in these samples; thus, a simple SSZ vs MORB discrimination diagram is inadequate. On all non-Th based discrimination diagrams (Figs. 6a and 8), the studied samples plot uniformly in the MORB field, while a Th-based discrimination plot suggests a crustal influence source (Figs. 7a and 9). Overall, the geochemical pattern suggests strong evidence of either an arc or MORB setting, with complications on both sides. Therefore, a possible interpretation that is largely consistent with the studied geochemical characters is the formation of these rocks in the early stages of rifting in a back-arc setting during slab-roll back, never developing into a true back-arc basin. This evidence is supported by the Ce/Nb–Th/Nb, Th/Yb–Nb/Yb and Ti–V, where the samples plot in the back-arc field.

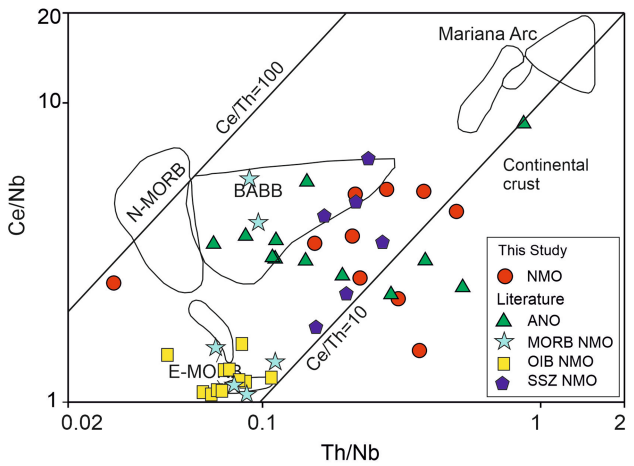

Fig. 9 Ce/Nb vs Th/Nb diagram from Saunders (1988). N-MORB= Depleted mid-ocean ridge, E-MORB= Enriched mid-ocean ridge basalt field, BABB=back-arc basin basalt field, CC= Continental Crust (from McLennan,2001)

It is widely assumed that the ophiolites of the eastern Indian plate (NMO and ANO) are part of the same subduction zone (Liu et al. 2016), as evidenced by the younging trend of these ophiolites in a southward direction and being part of the same fore-arc system. Considering the evolution and paleogeography of the Neotethyan, it is well established that an intra-ocean island arc existed within the Neotethys during the cretaceous period (Aitchison et al. 2000; Khan et al. 1997 2009). The island arc is suggested to be the Incertus-Woyla Arc (Hall 2012), which formed as early as 135 Ma (Bosch et al. 2011) or 150 Ma (Bouilhol et al. 2009) (Fig. 10). The development of the intra-oceanic arc was the result of divergent double subduction and led to the formation of a back-arc basin behind the Incertus-Woyla Arc (Barber et al. 2005; Advokaat et al. 2018; Plunder et al. 2020; Bandyopadhyay et al. 2021). This back-arc basin is a suitable candidate for the formation of the studied samples of NMO, as compared to a fore-arc rifting, which is difficult to fit in terms of the regional paleogeography of the Neotethyan. The formation and evolution of ANO in this back-arc setting are well recognized (Advokaat et al. 2018; Plunder et al 2020; Bandyopadhyay et al. 2021), where they conceptually explained the southward motion of a triple junction and the consumption of the Ngalau plate to produce the back-arc signature of ANO behind the Woyla Arc (~ 120 Ma). Although this paper does not have the new geochronological data from NMO, the similarity in the geochemical signatures with the ophiolite of ANO along with the published K–Ar isotopic age (148 ± 4 Ma) studies conducted from the NMO basalt (Sarkar et al. 1996) and concordant K–Ar age from radiolarian-bearing chert (Baxter et al. 2011) at 148 ± 4 Ma suggest an evolution of NMO corresponding to ANO in this back-arc setting. The isotopic age of NMO basalt of 148 ± 4 Ma by Sarkar et al. 1996 and chert age (Upper Jurassic) by Baxter et al. (2011) fit well into the formation of the Incertus-Woyla Arc at 150 Ma by Bouilhol et al. (2011). Earlier authors (Advokaat et al. 2018; Plunder et al. 2020; Bandyopadhyay et al. 2021) also supported the concept of the NMO and ANO developing in the back-setting behind the Incertus-Woyla Arc. However, Bandyopadhyay et al. 2021 also implied that the ophiolites of the NMO blocks might be

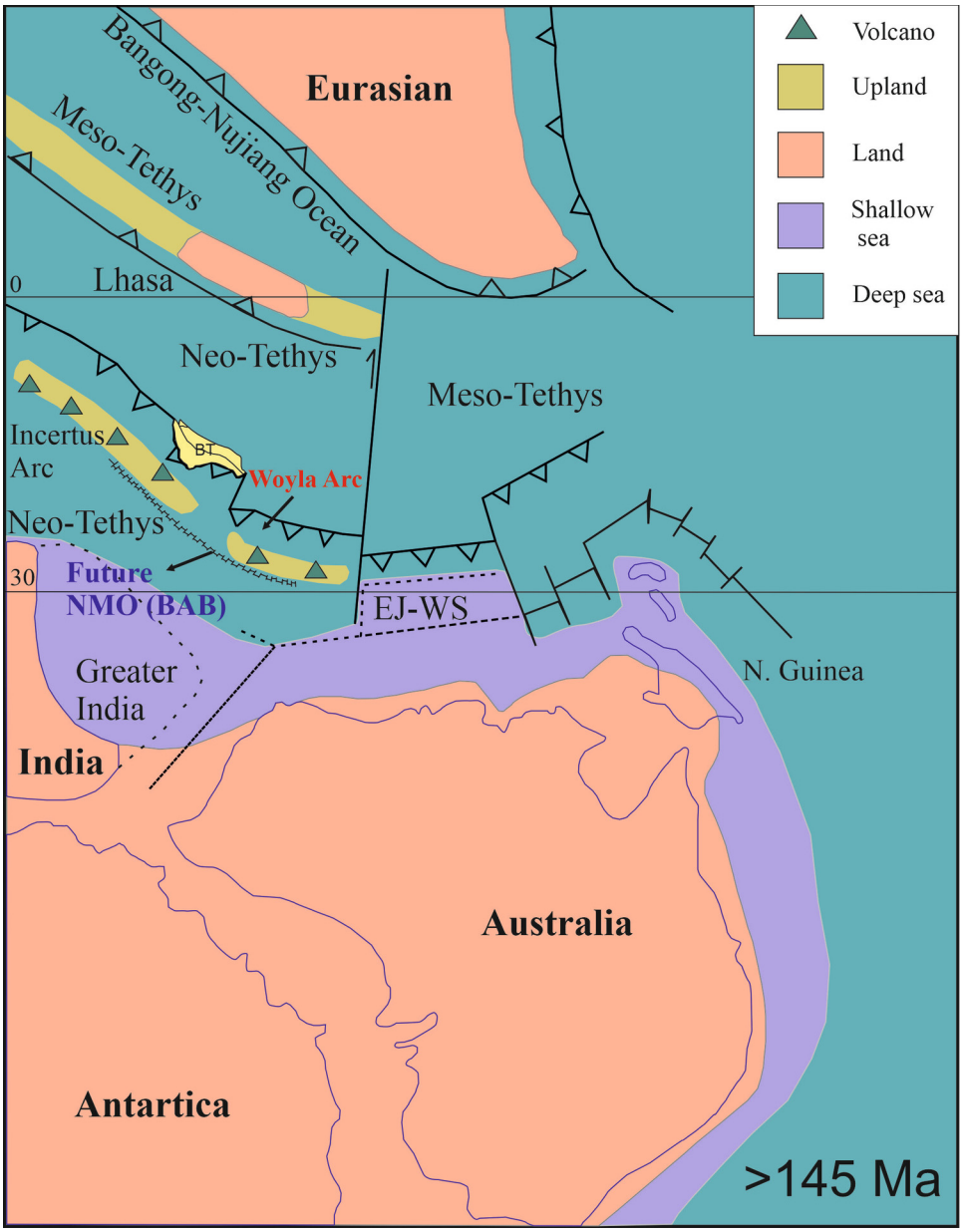

Fig. 10 Palaeogeographic reconstruction of eastern Tethys during 155 Ma-145 Ma modified after Metcalfe 2013 and Hall 2012. The Neo-tethyan opened in two stages, the western Neo-tethyan opened when the Lhasa block got separated from Gondwana Margin, while the eastern Neo-tethys opened when SW Borneo East Java-West Sulawesi (EJ-WS) separated from Australian Gondwana. The eastern Neo-tethyan was separated from the Meso-tethys by a major transform fault. The development of the Intra-oceanic arc (Incertus and Woyla Arc) and subsequent BAB (future site of NMO) within the Neo-tethyan during this time was a result of divergent double subduction (Norhteast Subduction along Euasian and Southwest subduction beneath the Incertus-woyla arc (Aitchison et al., 2000; Khan et al., 1997, 2009; Hall, 2012; Metcalfe 2013; Bouilhol et al., 2009; Advokaat et al 2018; Bandyopadhyay et al 2021; Plunder et al., 2020). BAB - Back-arc Basalt, SSZ - Supra Subduction Zone, OIB - Ocean Island Basalt, MORB-Midoceanic ridge basalt

of different plates compared with ANO. This comes after the recent paleomagnetic data by Westerweel et al. (2019), suggesting that the Indo-Burma ranges, along with Burma terrane, were located at the same latitude as Sumatra during the Cretaceous period. Based on the palaeomagnetic reconstruction by Westerweel et al. 2019, around 95 Ma, the Woyla Arc was accreting toward Eurasai (Westerweel et al. 2019; Plunder et al. 2020), while the Incertus Arc lay below the equatorial line divided by a transform fault between them. We thus speculate that the NMO might have been formed behind the Incertus Arc, while ANO was situated behind the Woyla Arc (Fig. 11).

A possible reconstruction of a back-arc rifting within the Neotethyan plate during the divergent double subduction is elaborated in Fig. 12. The subduction of the south-westward moving upper Neotethyan plate (Ngalau plate by Advokaat et al. 2018) generated the back-arc basin and the Incertus-Woyla Arc above the subduction zone (Fig. 10). The back-arc basalt of the eastern Indian plate ophiolite formed during the stage of slab roll-back, correlated with the oblique subducting slab to provide space for the asthenosphere to ascend. The architecture of the back-arc basalt melts progresses when the metasomatized fluids are released from, and along with the melting of the sinking oceanic crust interact with, the upwelling asthenosphere melt. Earlier studies show that the typical forearc SSZ mafic signatures registered from the ophiolite of NMO do not comply with the signature of this setting.

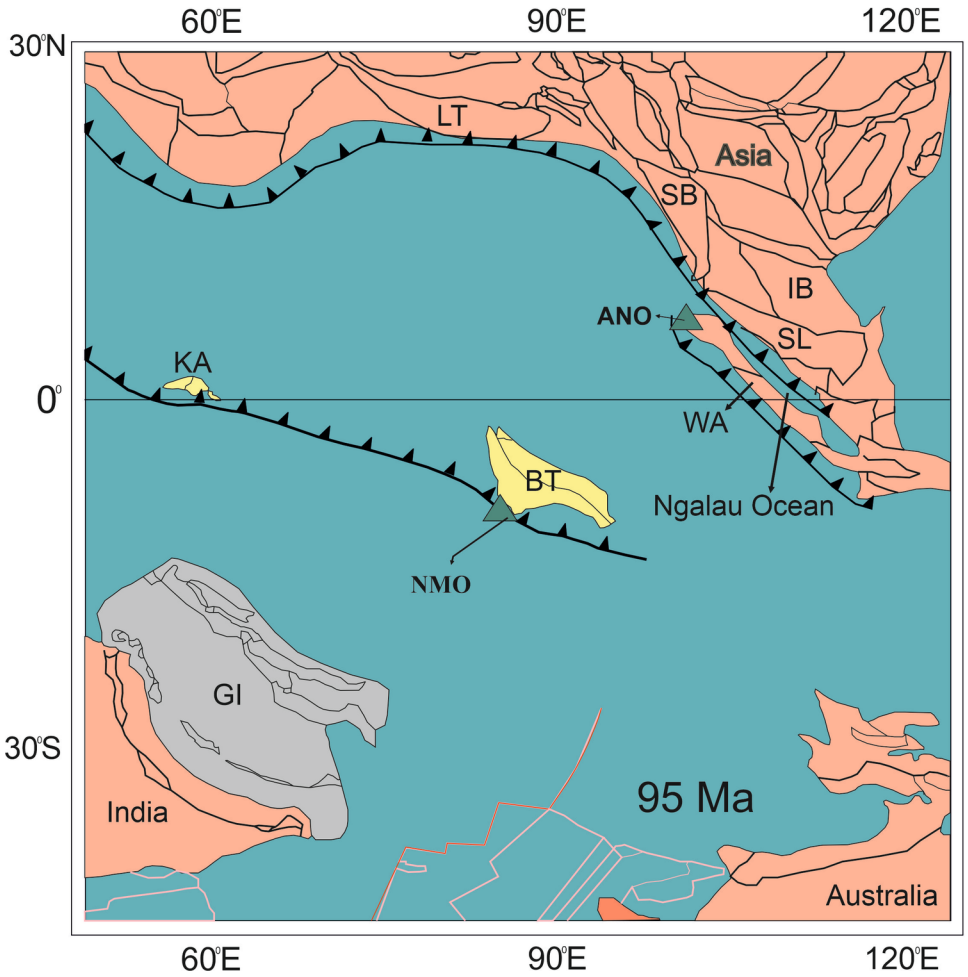

Fig. 11 India-Asia Palaeo-geography at 95 Ma modified after Westerweel et al.,2019. Kohistan Arc (KA) and Burma Terrane (BT) as segment of the Incertus Arc when Neo-Tethyan subduction began (Westerweel et al., 2019). In that period the BABB samples of NMO and were already accommodated with the segmented part of Incertus Arc. At approximately 95 Ma, most of the Woyla arc is accreted into Sundaland (Advokaat et al., 2018) with the commencement of Arc magmatism as attested by the agglomerates of ANO (Plunder et al., 2020). LT = Lhasa Tettane, IB = Indochina Block, GI = Greater India, SB = Simbumasu Block, SL = Sundaland Block, WA=Woyla Arc. Thin Pink lines represent Seafloor magnetic Isochrons of the present day, Red lines postulate Oceanic ridges and transform fault

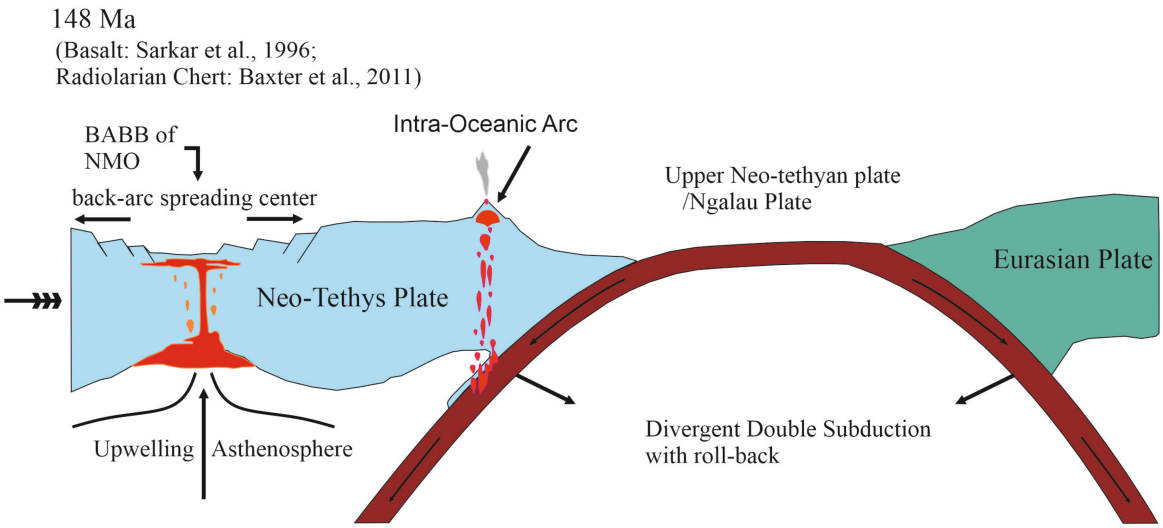

Fig. 12 Possible reconstruction for the evolution of BABB in NMO before subduction polarity reversal

Considering the results and the literature data (Singh et al. 2016; Khogenkumar et al. 2016; Akhtar et al. 2022; Bandyopadhyay et al. 2021) presented in this study, we postulate a revised scenario in which the back-arc and SSZ setting existed at different periods during the formation and evolution of NMO. At around 145 Ma the upper Neotethyan plate was consumed in a divergent double subduction system (Advokaat et al. 2018; Plunder et al 2020; Bandyopadhyay et al. 2021). The southwestern subduction of the Neotethyan plate created the intra-oceanic Incertus-Woyla Arc with the associated back-arc rifting and split the Neotethyan oceanic plate into two parts. This subduction is attested by the studied back-arc basalt and the published isotopic age of 148 ± 4 Ma by Sarkar et al. (1996) and Baxter et al. (2011) of NMO. In ANO, Advokaat et al. (2018) postulated that the subduction of the Upper Neotethyan plate below the Incertus-Woyla Arc was arrested in a later stage with subsequent subduction polarity reversal. Although we cannot evaluate when the subduction polarity reversal was initiated in NMO, the reversal led to the subduction initiation of the back-arc behind the Incertus-Woyla Arc. The developments of the metamorphic sole and gabbro (Plunder et al 2020; Bandyopadhyay et al. 2021) at 105 Ma of ANO represent the consequence of subduction initiation and the initial formation of ANO. In the context of NMO, the U–Pb zircon age of 116.4–118.8 Ma, formed plagiogranite (Singh et al. 2017a) and gabbro (Aitchison et al. 2019) with a SSZ signature represent a mature arc system after subduction polarity reversal. However, a mature arc of SSZ affinity in ANO is younger than NMO and is represented by plagiogranite (Jafri et al. 1990; Sarma et al. 2010) and agglomerate (Pederson et al. 2010) from between 93 and 95 Ma. This scenario finally leads to the closing of the Neotethyan when India and Eurasia collided at an equivocal age estimation of between 60 Ma (Yin 2010) and 35 Ma (Ali and Aitchison 2008; Aitchison and Ali 2007).

9 Conclusion

Considering the presented results and data from the literature, we propose the formation and evolution of Eastern Indian plate ophiolite, i.e., Nagaland-Manipur ophiolites (NMO) and Andaman-Nicobar ophiolites (ANO), as follows.

1. The mafic rocks of NMO show a sub-alkaline character with $Nb/Y < 0.40$, low Nb/Th 3.9 and low-to-moderate La/Sm (~ 1.72), indicating derivation from a slightly enriched mantle source in a mid-oceanic spreading setting. Their mid-oceanic basaltic affinity is supported by their enriched LREE pattern with flat HREE [$(La/Yb)_N = 1.72$] and higher TiO_2 abundances (average $TiO_2 = 1.21$ wt%). The magma source of the studied samples shows its derivation from 15 to 30% partial melting of a depleted mantle source of spinel-peridotite facies.
2. The geochemical characteristics of mafic rocks of the ANO are $Nb/Y < 0.40$, low Nb/Th 4.59, La/Sm 1.6, flat HREE [$(La/Yb)_N = 0.68–2.05$] and high TiO_2 up to 1.57 wt%. Both ANO and NMO exhibit depleted Nb and are enriched in U and Pb, suggesting a subduction influence during their generation. Recent geodynamic and paleogeographic reconstructions have suggested the existence of an ancient intra-oceanic arc and its associated back-arc system within the Neotethyan plate.
3. We found that the geochemical signatures of mafic rocks of NMO and ANO are comparable, and the available geochronology data of 145 Ma from the NMO basalt and chert fit well into the evolution and formation of the intra-oceanic arc, i.e., Incertus-Woyla Arc.
4. The evolution and formation of the back-arc basalt for the NMO is attributed to the southwest subduction of the Upper Neotethyan plate during divergent double subduction. This subduction resulted in the development of the intra-oceanic Incertus-Woyla Arc and its associated back-arc to which the isotopic age of 148 ± 4 Ma is assigned.
5. In the later stage, after the arrest of the Upper Neotethyan plate subduction and subsequent subduction polarity reversal, we interpret the U–Pb zircon age of 116.4–118.8 Ma from plagiogranite and gabbro with SSZ affinity to have formed in a mature arc system of the NMO.

Acknowledgements . This work is part of the doctoral research of the first author and partially supported by the Ministry of Earth Sciences (MoES), Government of India, New Delhi, through a research grant (No. MoES/P.O. (Geo)/80/2015) to A. K. Singh. Our sincere thanks are extended to all the authors whose published data are used in this article. The authors are grateful to the Editor and Editorial Director for their efficient editorial handling and two anonymous reviewers for their insightful comments.

Author contributions S. Imtisunep: Conceptualization, methodology, data curation, illustration, investigation, writing-original draft; A. Krishnakanta Singh: Supervision, conceptualization, methodology, data curation, investigation, writing-review & editing; Monika Chaubey: investigation, writing—review & editing; R.K. Bikrmaditya Singh: Supervision, investigation, writing—review & editing; Bendangtola Longchar: investigation, writing-review & editing; Shoraisam Khogenkumar: investigation, writing-review & editing; Amrita Dutt: investigation, writing—review & editing.

Declarations

Conflict of interest The authors declare that they have no known competing financial interests or personal relationships that could have appeared to influence the work reported in this paper. The authors alone are responsible for the content and writing of this article.

References

Acharyya SK (1986) Cenozoic plate motions creating the Eastern Himalayas and Indo-Burmese range around the North–East corner of India. In: Indian chapter IGCP Projects 195 and 197. Pp 143–161.

Advokaat EL, Bongers ML, Rudyawan A, BouDagher-Fadel MK, Langereis CG, van Hinsbergen DJJ (2018) Early Cretaceous origin of the Woyla arc (Sumatra, Indonesia) on the Australian plate. Earth Planet Sci Lett 498:348–361. https://doi.org/10.1016/j.epsl.2018.07.001

Agarwal OP, Ghosh NC (1986) Geology and stratigraphy of Naga ophiolite between Meluri and Awankho. Phek District, Nagaland, India. Tectonic context 105–30

Aitchison JC, Ali JR, Davis AM (2007) When and where did India and Asia collide? J Geophys Res Solid Earth 112(B5):B05423. https://doi.org/10.1029/2006JB004706

Aitchison JC, Davis AM, Liu J et al (2000) Remnants of a Cretaceous intra-oceanic subduction system within the Yarlung-Zangbo suture (southern Tibet). Earth Planet Sci Lett 183(1–2):231–44.

Aitchison JC, Ao A, Bhowmik S, Clarke GL, Ireland TR, Kachovich S, Lokho K, Stojanovic D, Roeder T, Truscott N, Zhen Y, Zhou RJ (2019) Tectonic evolution of the western margin of the Burma microplate based on new fossil and radiometric age constraints. Tectonics 38(5):1718–1741. https://doi.org/10.1029/2018tc005049

Akhtar S, Negi P, Saikia A (2021) Cumulate gabbros in the South Andaman Island ophiolite suite (India): their bearing on the tectonic setting. Can J Earth Sci 58(11):1170–1186. https://doi.org/10.1139/cjes-2020-0182

Akhtar S, Saikia A, Negi P, Kalita BJ (2022) Back-arc basin origin for the basalts of the South Andaman Island Ophiolite (India). Episodes 45(1):5–27. https://doi.org/10.18814/epiiugs/2021/021001

Ali JR, Aitchison JC (2008) Gondwana to Asia: Plate tectonics, paleogeography and the biological connectivity of the Indian sub-continent from the Middle Jurassic through latest Eocene (166–35 Ma). Earth Sci Rev 88(3–4):145–166. https://doi.org/10.1016/j.earscirev.2008.01.007

Allégre CJ, Courtillot V, Tapponnier P, Hirn A, Mattauer M, Coulon C, Jaeger JJ, Achache J, Schärer U, Marcoux J, Burg JP, Girardeau J, Armijo R, Gariépy C, Göpel C, Tindong L, Xiao XC, Chang CF, Li GQ, Lin BY, Teng JW, Wang NW, Chen GM, Han TL, Wang XB, Wanming D, Sheng HB, Cao YG, Zhou J, Qiu HR, Bao PS, Wang SC, Wang BX, Zhou YX, Xu RH (1984) Structure and evolution of the Himalaya–Tibet Orogenic Belt. Nature 307(5946):17–22. https://doi.org/10.1038/307017a0

Ao A, Bhowmik SK (2014) Cold subduction of the Neotethys: the metamorphic record from finely banded lawsonite and epidote blueschists and associated metabasalts of the Nagaland ophiolite complex, India. J Metamorph Geol 32(8):829–860. https://doi.org/10.1111/jmg.12096

Ao A, Satyanarayanan M (2022) Petrogenesis of mantle peridotite and cumulate peridotite rocks from the Nagaland Ophiolite Complex, NE, India. Geol J 57(2):749–767. https://doi.org/10.1002/gj.4314

Bandopadhyay PC (2012) Re-interpretation of the age and environment of deposition of Paleogene turbidites in the Andaman and Nicobar Islands, Western Sunda Arc. J Asian Earth Sci 45:126–137. https://doi.org/10.1016/j.jseaes.2011.08.018

Bandopadhyay PC (2005) Discovery of abundant pyroclasts in the Namunagarh Grit, south Andaman: evidence for arc volcanism and active subduction during the Palaeogene in the Andaman area. J Asian Earth Sci 25(1):95–107. https://doi.org/10.1016/j.jseaes.2004.01.007

Bandyopadhyay D, Ghosh B, Guilmette C, Plunder A, Corfu F, Advokaat EL, Bandopadhyay PC, van Hinsbergen DJJ (2021) Geochemical and geochronological record of the Andaman Ophiolite, SE Asia: from back-arc to forearc during subduction polarity reversal? Lithos 380:105853. https://doi.org/10.1016/j.lithos.2020.105853

Barber AJ, Crow MJ, Milsom J (eds) (2005) Sumatra: Geology, resources and tectonic evolution. Geological Society of London, London.

Baxter AT, Aitchison JC, Zyabrev SV, Ali JR (2011) Upper Jurassic radiolarians from the Naga ophiolite, Nagaland, northeast India. Gondwana Res 20(2–3):638–644.

Bhattacharya S, Pande K, Kumar A, Kingson O, Ray JS, (2020) Timing of formation and obduction of the Andaman ophiolite. The Andaman Islands and Adjoining Offshore. Geology, Tectonics and Palaeoclimate, pp 19–42.

Beccaluva L, Macciotta G, Piccardo GB, Zeda O (1989) Clinopyroxene composition of ophiolite basalts as petrogenetic indicator. Chem Geol 77(3–4):165–182. https://doi.org/10.1016/0009-2541(89)90073-9

Bhowmik SK, Ao A (2016) Subduction initiation in the Neo-Tethys: constraints from counterclockwise *P-T* paths in amphibolite rocks of the Nagaland Ophiolite Complex, India. J Metamorph Geol 34(1):17–44. https://doi.org/10.1111/jmg.12169

Bosch D, Garrido CJ, Bruguier O et al (2011) Building an island-arc crustal section: Time constraints from a LA-ICP-MS zircon study. Earth Planet Sci Lett 309(3–4):268–279.

Bouilhol P, Burg JP, Bodinier JL et al (2009) Magma and fluid percolation in arc to forearc mantle: evidence from Sapat (Kohistan, Northern Pakistan). Lithos 107(1–2):17–37.

Bouilhol P, Schaltegger U, Chiaradia M, Ovtcharova M, Stracke A, Burg JP, Dawood H (2011) Timing of juvenile arc crust formation and evolution in the Sapat Complex (Kohistan–Pakistan). Chem Geol 280(3–4):243–256. https://doi.org/10.1016/j.chemgeo.2010.11.013

Brunnschweiler RO (1966) On the geology of the Indo Burman ranges Arakan Coast and Yoma, Chin Hills, Naga Hills. J Geol Soc Aust 13(1):137–194. https://doi.org/10.1080/00167616608728608

Chakraborty PP, Pal T (2001) Anatomy of a forearc submarine fan: Upper Eocene—Oligocene Andaman Flysch Group, Andaman Islands. India Gondwana Res 4(3):477–486. https://doi.org/10.1016/S1342-937X(05)70347-6

Chaubey M, Singh AK, Singh BP, Imtisunep S et al (2022) Refertilization of depleted mantle peridotite in the Nagaland-Manipur ophiolite, north-east India: Constraints from PGE, mineral, and whole-rock geochemistry. Geol J 57(12):5265–5283.

Chaubey M, Singh AK, Imtisunep S, Uysal I, Singh BP, Satyanarayanan M, Longchar B, Khogenkumar S (2024) Formation of the associating high-Al and high-Cr chromitites in the Nagaland–Manipur Ophiolites in northeast India. Int Geol Rev. https://doi.org/10.1080/00206814.2024.2386565

Chemenda AI, Yang RK, Stephan JF, Konstantinovskaya EA, Ivanov GM (2001) New results from physical modelling of arc–continent collision in Taiwan: evolutionary model. Tectonophysics 333(1–2):159–178. https://doi.org/10.1016/S0040-1951(00)00273-0

Chungkham P, Jafar SA (1998) Late Cretaceous (Santonian–Maastrichtian) integrated coccolith-globotruncanid biostratigraphy of pelagic limestones from the accretionary prism of Manipur, Northeastern India. Micropaleontology 1:69–83.

Condie KC (1989) Geochemical changes in basalts and andesites across the Archean-Proterozoic boundary: identification and significance. Lithos 23(1–2):1–18. https://doi.org/10.1016/0024-4937(89)90020-0

Dai JG, Wang CS, Li YL (2012) Relicts of the Early Cretaceous seamounts in the central-western Yarlung Zangbo Suture Zone, southern Tibet. J Asian Earth Sci 53:25–37. https://doi.org/10.1016/j.jseaes.2011.12.024

Dai JG, Wang CS, Polat A, Santosh M, Li YL, Ge YK (2013) Rapid forearc spreading between 130 and 120 Ma: evidence from geochronology and geochemistry of the Xigaze ophiolite, southern Tibet. Lithos 172:1–16. https://doi.org/10.1016/j.lithos.2013.03.011

Davidson JP (1987) Crustal contamination versus subduction zone enrichment: examples from the lesser Antilles and implications for mantle source compositions of island arc volcanic rocks. Geochim Cosmochim Acta 51(8):2185–2198. https://doi.org/10.1016/0016-7037(87)90268-7

Davies JH, von Blanckenburg F (1995) Slab breakoff: A model of lithosphere detachment and its test in the magmatism and deformation of collisional orogens. Earth Planet Sci Lett 129(1–4):85–102.

Dilek Y, Furnes H (2009) Structure and geochemistry of Tethyan ophiolites and their petrogenesis in subduction rollback systems. Lithos 113(1–2):1–20. https://doi.org/10.1016/j.lithos.2009.04.022

Dilek Y, Furnes H (2011) Ophiolite genesis and global tectonics: geochemical and tectonic fingerprinting of ancient oceanic lithosphere. Geol Soc Am Bull 123(3–4):387–411. https://doi.org/10.1130/B30446.1

Dilek Y, Newcomb S (2003) Ophiolite concept and its evolution. In: Ophiolite concept and the evolution of geological thought. Geological Society of America, pp 1–16. https://doi.org/10.1130/0-8137-2373-6.1

Dewey JF (1976) Ophiolite obduction. Tectonophysics 31(1–2):93–120. https://doi.org/10.1016/0040-1951(76)90169-4

Dubois-Côté V, Hébert R, Dupuis C, Wang CS, Li YL, Dostal J (2005) Petrological and geochemical evidence for the origin of the Yarlung Zangbo ophiolites, southern Tibet. Chem Geol 214(3–4):265–286. https://doi.org/10.1016/j.chemgeo.2004.10.004

Dutt A, Singh AK, Srivastava RK, Oinam G (2021a) Evidence of melt–and fluid–rock interactions in the refractory forearc peridotites and associated mafic intrusives from the Tuting-Tidding ophiolites, eastern Himalaya, India: petrogenetic and tectonic implications. Geol J 56(4):2082–2110. https://doi.org/10.1002/gj.4043

Dutt A, Singh AK, Srivastava RK, Oinam G, Bikramaditya RK (2021b) Geochemical and metamorphic record of the amphibolites from the Tuting-Tidding Suture zone ophiolites, eastern Himalaya, India: implications for the presence of a dismembered metamorphic sole. Geol Mag 158(5):787–810. https://doi.org/10.1017/s0016756820000825

Faccenda M, Gerya TV, Chakraborty S (2008) Styles of post-subduction collisional orogeny: influence of convergence velocity, crustal rheology and radiogenic heat production. Lithos 103(1–2):257–287. https://doi.org/10.1016/j.lithos.2007.09.009

Ferrari L (2004) Slab detachment control on mafic volcanic pulse and mantle heterogeneity in central Mexico. Geology 32(1):77. https://doi.org/10.1130/g19887.1

Furnes H, Dilek Y, Pedersen RB (2012) Structure, geochemistry, and tectonic evolution of trench-distal backarc oceanic crust in the western Norwegian Caledonides, Solund-Stavfjord ophiolite (Norway). Geol Soc Am Bull 124(7–8):1027–1047. https://doi.org/10.1130/b30561.1

Ghose NC, Agrawal OP, Chatterjee N (2010) Geological and mineralogical study of eclogite and glaucophane schists in the Naga Hills Ophiolite. Northeast India Isl Arc 19(2):336–356. https://doi.org/10.1111/j.1440-1738.2010.00710.x

Ghose NC, Shrivastava MP (1986) Podiform chromites of Naga hills ophiolites NE, India. In: Chromites. Thophuastus Publications, Athens. pp 263–284.

Ghose NC, Singh RN (1980) Occurrence of blueschist facies in the ophiolite belt of Naga Hills, east of Kiphire, NE India. Geol Rundsch 69:41–48.

Ghosh B, Morishita T, Bhatta K (2013) Significance of chromian spinels from the mantle sequence of the Andaman ophiolite, India: paleogeodynamic implications. Lithos 164:86–96. https://doi.org/10.1016/j.lithos.2012.08.004

Ghosh B, Mukhopadhyay S, Morishita T, Tamura A, Arai S, Bandyopadhyay D, Chattopadhaya S, Ovung TN (2018) Diversity and evolution of suboceanic mantle: constraints from Neotethyan ophiolites at the eastern margin of the Indian plate. J Asian Earth Sci 160:67–77. https://doi.org/10.1016/j.jseaes.2018.04.010

Girardeau J, Mercier JCC, Wang XB (1985a) Petrology of the mafic rocks of the Xigaze ophiolite, Tibet: implications for the genesis of the oceanic lithosphere. Contrib Mineral Petrol 90(4):309–321. https://doi.org/10.1007/BF00384710

Girardeau J, Mercier JCC, Yougong Z (1985b) Origin of the Xigaze ophiolite, Yarlung Zangbo suture zone, southern Tibet. Tectonophysics 119(1–4):407–433. https://doi.org/10.1016/0040-1951(85)90048-4

Guruaribam V, Singh YR, Singh AK (2022) Age and depositional environment of carbonate exotics associated with the Disang group of Assam-Arakan Basin, northeast India: constraints from microfossils and geochemistry. Carbonates Evaporites 36(3):46. https://doi.org/10.1007/s13146-021-00715-8

Gururajan NS, Choudhuri BK (2003) Geology and tectonic history of the Lohit Valley, Eastern Arunachal Pradesh. India J Asian Earth Sci 21(7):731–741. https://doi.org/10.1016/S1367-9120(02)00040-8

Haldar D (1985) Some aspects of the Andaman Ophiolite Complex. Rec Geol Surv Ind 115:1–11.

Hall R (2012) Late Jurassic-Cenozoic reconstructions of the Indonesian Region and the Indian Ocean. Tectonophysics 570:1–41. https://doi.org/10.1016/j.tecto.2012.04.021

Harris NBW, Pearce JA, Tindle AG (1986) Geochemical characteristics of collision-zone magmatism. Geol Soc Lond Spec Publ 19(1):67–81. https://doi.org/10.1144/gsl.sp.1986.019.01.04

Hofmann AW (1988) Chemical differentiation of the earth: the relationship between mantle, continental crust andoceanic crust. Earth Planet Sci Lett 90: 297–314

Imtisunep S, Singh AK, Bikramaditya R, Khogenkumar S, Chaubey M, Kumar N (2022) Evidence of intraplate magmatism and subduction magmatism during the formation of Nagaland-Manipur Ophiolites, Indo–Myanmar Orogenic Belt, north-east India. Geol J 57(2):782–800. https://doi.org/10.1002/gj.4378

Jafri SH, Sheikh JM (2013) Geochemistry of pillow basalts from Bompoka, Andaman–Nicobar Islands, Bay of Bengal, India. J Asian Earth Sci 64:27–37. https://doi.org/10.1016/j.jseaes.2012.11.035

Jafri SH, Balaram V, Ramesh SL (1990) Geochemistry of Andaman–Nicobar island basalts: a case for a possible plume origin. J Volcanol Geotherm Res 44(3–4):339–347. https://doi.org/10.1016/0377-0273(90)90026-C

Khan MA, Stern RJ, Gribble RF, Windley BF (1997) Geochemical and isotopic constraints on subduction polarity, magma sources, and palaeogeography of the Kohistan intra-oceanic arc, northern Pakistan Himalaya. J Geol Soc 154(6):935–946.

Khan SD, Walker DJ, Hall SA et al (2009) Did the Kohistan-Ladakh island arc collide first with India? Geol Soc Am Bull 121(3–4):366–384.

Khogenkumar S, Singh AK, Kumar S, Lakhan N, Chaubey M, Imtisunep S, Dutt A, Oinam G (2021) Subduction versus non-subduction origin of the Nagaland–Manipur ophiolites along the Indo–Myanmar orogenic belt, northeast India: fact and fallacy. Geol J 56(4):1773–1794. https://doi.org/10.1002/gj.4030

Khogenkumar S, Singh AK, Bikramaditya Singh RK, Khanna PP, Singh NI, Singh WI (2016) Coexistence of MORB and OIB-type mafic volcanics in the Manipur Ophiolite Complex, Indo–Myanmar Orogenic Belt, northeast India: implication for heterogeneous mantle source at the spreading zone. J Asian Earth Sci 116:42–58. https://doi.org/10.1016/j.jseaes.2015.11.007

Kingson O, Bhutani R, Balakrishnan S, Dash JK, Shukla AD (2019) Subduction-related Manipur Ophiolite Complex, Indo–Myanmar Ranges: elemental and isotopic record of mantle metasomatism. Geol Soc Lond Spec Publ 481(1):195–210. https://doi.org/10.1144/sp481.9

Leat PT, Livermore RA, Millar IL, Pearce JA (2000) Magma supply in back-arc spreading centre segment E2, East Scotia Ridge. J Petrol 41(6):845–866.

Leeman WP (2020) Old/New subduction zone paradigms as seen from the Cascades. Front Earth Sci 8:419. https://doi.org/10.3389/feart.2020.535879

Leterrier J, Maury RC, Thonon P, Girard D, Marchal M (1982) Clinopyroxene composition as a method of identification of the magmatic affinities of paleo-volcanic series. Earth Planet Sci Lett 59(1):139–154. https://doi.org/10.1016/0012-821X(82)90122-4

Levander A, Bezada MJ, Niu F, Humphreys ED, Palomeras I, Thurner SM, Masy J, Schmitz M, Gallart J, Carbonell R, Miller MS (2014) Subduction-driven recycling of continental margin lithosphere. Nature 515(7526):253–256. https://doi.org/10.1038/nature13878

Licht A, Dupont-Nivet G, Win Z et al (2019) Paleogene evolution of the Burmese forearc basin and implications for the history of India-Asia convergence. GSA Bull 131(5–6):730–748.

Liu CZ, Chung SL, Wu FY et al (2016) Tethyan suturing in Southeast Asia: Zircon U-Pb and Hf-O isotopic constraints from Myanmar ophiolites. Geology 44(4):311–314.

Maibam B, Foley S, Luguet A, Jacob DE, Singh TB, Ray D, Panda DK, Keppler R (2017) Characterisation of chromites, chromite hosted inclusions of silicates and metal alloys in chromitites from the Indo–Myanmar ophiolite belt of Northeastern India. Ore Geol Rev 90:260–273. https://doi.org/10.1016/j.oregeorev.2017.05.032

McLennan SM (2001) Relationships between the trace element composition of sedimentary rocks and upper continental crust. Geochem Geophys Geosyst 2(4):1021. https://doi.org/10.1029/2000GC000109

Metcalfe I (2013) Gondwana dispersion and Asian accretion: tectonic and palaeogeographic evolution of eastern Tethys. J Asian Earth Sci 66:1–33. https://doi.org/10.1016/j.jseaes.2012.12.020

Morimoto N, Fabries J, Ferguson AK et al (1989) Nomenclature of pyroxenes. subcommittee on pyroxenes. Commission on new minerals and mineral names. Can Mineral 27:143–156.

Murton BJ (1989) Tectonic controls on boninite genesis. Geol Soc Lond Spec Publ 42(1):347–377. https://doi.org/10.1144/gsl.sp.1989.042.01.20

Nicolas A, Girardeau J, Marcoux J, Dupre B, Wang XB, Cao YG, Zheng HX, Xiao XC (1981) The Xigaze ophiolite (Tibet): a peculiar oceanic lithosphere. Nature 294(5840):414–417. https://doi.org/10.1038/294414a0

Ningthoujam PS, Dubey CS, Guillot S, Fagion AS, Shukla DP (2012) Origin and serpentinization of ultramafic rocks of Manipur Ophiolite Complex in the Indo–Myanmar subduction zone, Northeast India. J Asian Earth Sci 50:128–140. https://doi.org/10.1016/j.jseaes.2012.01.004

Oldham RD (1885) Notes on the geology of Andaman Islands. Record Geol Surv India 18:135–145.

Pal T (2011) Petrology and geochemistry of the Andaman ophiolite: melt–rock interaction in a suprasubduction-zone setting. J Geol Soc 168(4):1031–1045. https://doi.org/10.1144/0016-76492009-152

Pal T, Chakraborty PP, Gupta TD, Singh CD (2003) Geodynamic evolution of the outer-arc–forearc belt in the Andaman Islands, the central part of the Burma-Java subduction complex. Geol Mag 140(3):289–307. https://doi.org/10.1017/s0016756803007805

Pal T, Bhattacharya A, Nagendran G, Yanthan NM, Singh R, Raghumani N (2014) Petrogenesis of chromites from the Manipur ophiolite belt, NE India: evidence for a suprasubduction zone setting prior to Indo–Myanmar collision. Mineral Petrol 108(5):713–726. https://doi.org/10.1007/s00710-014-0320-z

Parlak O, Dunkl I, Karaoğlan F, Kusky TM, Zhang C, Wang L, Koepke J, Billor Z, Hames WE, Şimşek E, Şimşek G, Şimşek T, Öztürk SE (2019) Rapid cooling history of a Neotethyan ophiolite: evidence for contemporaneous subduction initiation and metamorphic sole formation. GSA Bull 131(11–12):2011–2038. https://doi.org/10.1130/b35040.1

Pearce JA (1983) Role of the sub-continental lithosphere in magma genesis at active continental margins. In: Hawkesworth CJ and Norry MJ (eds) Continental basalts and mantle xenoliths, pp 230–249

Pearce JA, Stern RJ, Bloomer SH, Fryer P (2005) Geochemical mapping of the Mariana arc-basin system: implications for the nature and distribution of subduction components. Geochem Geophys Geosyst 6(7)

Pearce JA (2014) Immobile element fingerprinting of ophiolites. Elements 10(2):101–108. https://doi.org/10.2113/gselements.10.2.101

Pearce JA (2008) Geochemical fingerprinting of oceanic basalts with applications to ophiolite classification and the search for Archean oceanic crust. Lithos 100(1–4):14–48. https://doi.org/10.1016/j.lithos.2007.06.016

Pedersen RB, Searle MP, Carter A, Bandopadhyay PC (2010) U-Pb zircon age of the Andaman ophiolite: Implications for the beginning of subduction beneath the Andaman–Sumatra arc. J Geol Soc 167(6):1105–1112. https://doi.org/10.1144/0016-76492009-151

Perfit MR, Gust DA, Bence AE et al (1980) Chemical characteristics of island-arc basalts: implications for mantle sources. Chem Geol 30(3):227–256

Pilet S, Abe N, Rochat L, Kaczmarek MA, Hirano N, Machida S, Buchs D, Baumgartner P, Müntener O (2016) Pre-subduction metasomatic enrichment of the oceanic lithosphere induced by plate flexure. Nat Geosci 9:898–903. https://doi.org/10.1038/ngeo2825

Plunder A, Bandyopadhyay D, Ganerød M, Advokaat EL, Ghosh B, Bandopadhyay P, van Hinsbergen DJJ (2020) History of subduction polarity reversal during arc-continent collision: constraints from the Andaman ophiolite and its metamorphic sole. Tectonics 39(6):e2019TC005762. https://doi.org/10.1029/2019TC005762

Premi K, Sen AK, Singh AK, Lakhan N (2022) Petrogenesis and tectonic environments for formation of peridotites and associated podiform chromite ore, southern part of Manipur Ophiolite Belt, Indo–Myanmar Orogenic Belt, NE India. J Mineral Geochem 197(3):209–232. https://doi.org/10.1127/njma/2021/0255

Premi K, Sen AK, Singh AK, Singh WI, Chaubey M (2023) The genesis of peridotite-hosted podiform chromite ore and associated PGE, southern Manipur ophiolite complex northeast India. Periodico di Mineralogia. https://doi.org/10.13133/2239-1002/17854

Pysklywec RN (2001) Evolution of subducting mantle lithosphere at a continental plate boundary. Geophys Res Lett 28(23):4399–4402. https://doi.org/10.1029/2001gl013567

Ray KK, Sengupta S, Van Den Hul HJ (1988) Chemical characters of volcanic rocks from Andaman ophiolite. India J Geol Soc 145(3):393–400. https://doi.org/10.1144/gsjgs.145.3.0393

Ray JS, Pande K, Bhutani R (2015) $^{40}Ar/^{39}Ar$ geochronology of subaerial lava flows of Barren Island volcano and the deep crust beneath the Andaman Island Arc, Burma Microplate. Bull Volcanol 77(6):57. https://doi.org/10.1007/s00445-015-0944-9

Roy SK (1992) Accretionary prism in Andaman Forearc. Geolog Surv India Spec Publ 29:273–278.

Rudnick RL (2005) Composition of the continental crust. Crust Treatise Geochem 3:17–18.

Saha A, Dhang A, Ray J, Chakraborty S, Moecher D (2010) Complete preservation of ophiolite suite from south Andaman, India: a

mineral-chemical perspective. J Earth Syst Sci 119(3):365–381. https://doi.org/10.1007/s12040-010-0017-6

Saha A, Mudholkar AV, Kamesh Raju KA, Doley B, Sensarma S (2019) Geochemical characteristics of basalts from Andaman subduction zone: implications on magma genesis at intraoceanic back-arc spreading centres. Geol J 54(6):3489–3508. https://doi.org/10.1002/gj.3345

Sarkar A, Datta AK, Poddar BC, Bhattacharyya BK et al (1996) Geochronological studies of Mesozoic igneous rocks from eastern India. J SE Asian Earth Sci 13(2):77–81.

Sarma DS, Jafri SH, Fletcher IR, McNaughton NJ (2010) Constraints on the tectonic setting of the andaman ophiolites, Bay of Bengal, India, from SHRIMP U-Pb zircon geochronology of plagiogranite. J Geol 118(6):691–697. https://doi.org/10.1086/656354

Sengupta S, Acharyya SK, Van Den Hul HJ, Chattopadhyay B (1989) Geochemistry of volcanic rocks from the Naga Hills Ophiolites, northeast India and their inferred tectonic setting. J Geol Soc 146(3):491–498. https://doi.org/10.1144/gsjgs.146.3.0491

Sengupta S, Ray KK, Acharyya SK, De Smeth JB (1990) Nature of ophiolite occurrences along the eastern margin of the Indian plate and their tectonic significance. Geology 18(5):439–442.

Shervais JW (1982) Ti-V plots and the petrogenesis of modern and ophiolitic lavas. Earth Planet Sci Lett 59(1):101–118. https://doi.org/10.1016/0012-821X(82)90120-0

Singh AK (2009) High-Al chromian spinel in peridotites of Manipur Ophiolite Complex, Indo–Myanmar Orogenic Belt: Implication for petrogenesis and geotectonic setting. Curr Sci 96(7):973–978.

Singh AK (2013) Petrology and geochemistry of Abyssal Peridotites from the Manipur Ophiolite Complex, Indo–Myanmar Orogenic Belt, Northeast India: implication for melt generation in mid-oceanic ridge environment. J Asian Earth Sci 66:258–276. https://doi.org/10.1016/j.jseaes.2013.02.004

Singh AK, Singh NI, Devi LD, Bikramaditya Singh RK (2008) Pillow basalts from the Manipur ophiolitic complex (MOC), Indo–Myanmar range, northeast India. J Geol Soc Ind 72(2):168–174.

Singh AK, Khogenkumar S, Singh LR, Bikramaditya RK, Khuman CM, Thakur SS (2016) Evidence of Mid-ocean ridge and shallow subduction forearc magmatism in the Nagaland–Manipur ophiolites, northeast India: constraints from mineralogy and geochemistry of gabbros and associated mafic dykes. Geochemistry 76(4):605–620. https://doi.org/10.1016/j.chemer.2016.09.002

Singh AK, Devi LD, Singh NI, Subramanyam KSV, Bikramaditya Singh RK, Satyanarayanan M (2013) Platinum-group elements and gold distributions in peridotites and associated podiform chromitites of the Manipur Ophiolitic Complex, Indo–Myanmar Orogenic Belt, Northeast India. Geochemistry 73(2):147–161. https://doi.org/10.1016/j.chemer.2012.07.004

Singh AK, Chung SL, Bikramaditya RK, Lee HY (2017a) New U-Pb zircon ages of plagiogranites from the Nagaland–Manipur Ophiolites, Indo–Myanmar Orogenic Belt, NE India. J Geol Soc 174(1):170–179. https://doi.org/10.1144/jgs2016-048

Singh AK, Nayak R, Khogenkumar S, Subramanyam KSV, Thakur SS, Bikramaditya Singh RK, Satyanarayanan M (2017b) Genesis and tectonic implications of cumulate pyroxenites and tectonite peridotites from the Nagaland–Manipur ophiolites, northeast India: constraints from mineralogical and geochemical characteristics. Geol J 52(3):415–436. https://doi.org/10.1002/gj.2769

Singh AK, Chung S, Somerville I (2022a) Petrogenesis of mantle peridotites in Neo-Tethyan ophiolites from the Eastern Himalaya and Indo–Myanmar Orogenic Belt in the geotectonic framework of Southeast Asia. Geol J 57:4886–4919. https://doi.org/10.1002/gj.4629

Singh AK, Guruaribam V, Singh YR, Singh NI, Singh LR, Chaubey M, Tewari VC, Singh WI, Lakhan N, Devi LD, Chanu RS (2022b) Stable isotope geochemistry and microfossil assemblages of carbonate rocks in the ophiolite mélange zone of the Indo–Myanmar orogenic Belt, NE India: implications on age and depositional environment. Geol J 57(12):5308–5325. https://doi.org/10.1002/gj.4550

Srivastava RK, Chandra R, Shastry A (2004) High-Ti type N-MORB parentage of basalts from the south Andaman ophiolite suite. India J Earth Syst Sci 113(4):605–618. https://doi.org/10.1007/BF02704025

Stern RJ (2004) Subduction initiation: spontaneous and induced. Earth Planet Sci Lett 226(3–4):275–292. https://doi.org/10.1016/j.epsl.2004.08.007

Sun SS, McDonough WF (1989) Chemical and isotopic systematics of oceanic basalts: implications for mantle composition and processes. Geol Soc Lond Spec Publ 42(1):313–345. https://doi.org/10.1144/GSL.SP.1989.042.01.19

Tapponnier P, Mercier JL, Proust F, Andrieux J, Armijo R, Bassoullet JP, Brunel M, Burg JP, Colchen M, Dupré B, Girardeau J, Marcoux J, Mascle G, Matte P, Nicolas A, Li TD, Xiao XC, Chang CF, Lin PY, Li GC, Wang NW, Chen GM, Han TL, Wang XB, Wanming D, Zhen HX, Sheng HB, Yongong C, Zhou J, Qiu HR (1981) The Tibetan side of the India–Eurasia collision. Nature 294(5840):405–410. https://doi.org/10.1038/294405a0

Venkatramana P, Datta AK, Acharyya SK (1986) Petrography and petrochemistry of the ophiolite suite. Mem Geol Surv India 119:33–634.

Verencar A, Saha A, Ganguly S, Satyanarayanan M, Doley B, Ram Mohan M (2022) Multistage melt impregnation in Tethyan oceanic mantle: petrochemical constraints from channelized melt flow in the Naga Hills Ophiolite. Geochemistry 82(1):125821. https://doi.org/10.1016/j.chemer.2021.125821

Westerweel J, Roperch P, Licht A, Dupont-Nivet G, Win Z, Poblete F, Ruffet G, Swe HH, Thi MK, Aung DW (2019) Burma Terrane part of the Trans-Tethyan Arc during collision with India according to palaeomagnetic data. Nat Geosci 12(10):863–868. https://doi.org/10.1038/s41561-019-0443-2

Whattam SA, Stern RJ (2011) The 'subduction initiation rule': a key for linking ophiolites, intra-oceanic forearcs, and subduction initiation. Contrib Mineral Petrol 162(5):1031–1045. https://doi.org/10.1007/s00410-011-0638-z

Winchester JA, Floyd PA (1977) Geochemical discrimination of different magma series and their differentiation products using immobile elements. Chem Geol 20:325–343. https://doi.org/10.1016/0009-2541(77)90057-2

Yang GX (2022) Subduction initiation triggered by collision: a review based on examples and models. Earth Sci Rev 232:104129. https://doi.org/10.1016/j.earscirev.2022.104129

Yin A (2010) Cenozoic tectonic evolution of Asia: a preliminary synthesis. Tectonophysics 488(1–4):293–325. https://doi.org/10.1016/j.tecto.2009.06.002

Zaccarini F, Singh AK, Garuti G (2016) Platinum Group minerals and silicate inclusions in chromitite from the Naga–Manipur ophiolite complex, Indo–Myanmar orogenic belt, northeast India. Can Mineral 54(2):409–427. https://doi.org/10.3749/canmin.1500034